Physics 4P06

"Bifurcation of Bloch Waves in the Gross-Pitaevskii Equation"

Matthew Coles[1,2]
Supervisor: Dmitry Pelinovsky[1]

[1] *Department of Mathematics and Statistics, McMaster University, Hamilton, Ontario, Canada L8S 4K1*

[2] *Department of Physics and Astronomy, McMaster University, Hamilton, Ontario, Canada L8S 4M1*

April 21, 2011

Abstract

Stationary Bloch waves are considered in the Gross-Pitaevskii equation with a periodic potential for varying strengths of inter-atomic interactions. Upon a sufficient increase of the inter-atomic interactions one may observe a bifurcation in the number and stability of stationary states. This bifurcation generates loops in the energy bands of the Bloch waves near the ends and the center of the Brillouin zone. Using the method of Lyapunov-Schmidt reductions, the behaviour of stationary states is established close to the linear limit and around the bifurcation value. In particular, the bifurcation for the lowest energy band is shown to be a supercritical pitchfork bifurcation. The change in stability of the stationary states is also examined across the bifurcation point. Analytical results are illustrated by numerical computations for the lowest and excited energy bands.

1 Introduction

Let us consider the mean-field model for Bose-Einstein condensation, the Gross-Pitaevskii equation, in the space of one dimension,

$$i\frac{\partial \Psi}{\partial t} = -\frac{\partial^2 \Psi}{\partial x^2} + V(x)\Psi + c|\Psi|^2\Psi, \tag{1}$$

where $\Psi(x,t) : \mathbb{R} \times \mathbb{R} \to \mathbb{C}$ is the wave function of the condensate (with $|\Psi|^2$ being a probability density of Bose atoms), $V(x) : \mathbb{R} \to \mathbb{R}$ models the trapping mechanism, and $c \in \mathbb{R}$ models the strength of the inter-atomic interactions. The one-dimensional equation corresponds to the cigar shaped Bose-Einstein condensate.

We take the potential to be a 2π-periodic function; $V(x + 2\pi) = V(x)$. This potential corresponds to an optical lattice used for trapping the condensate. We deal both with the defocusing, $c > 0$, and focusing, $c < 0$, cases. The main interest that draws our attention is the possibility of loops in the energy bands associated with the nonlinear Bloch waves. This possibility was first discovered by Wu & Niu (see their review in [3]) and later explored numerically by Machholm, Pethick, and Smith [4]. The loops were discovered in the defocusing case, $c > 0$, for the lowest energy band near the end of the Brillouin zone and for the second energy band near the center of the Brillouin zone (see Figure 1 in [4]). For $V(x) = \cos(x)$, an analytical example of the new solutions bifurcating from the anti-periodic Bloch waves for the lowest energy band at $c = 1$ and existing for $c > 1$ is constructed by Bronski et al. [2].

More recently, a possibility of loops in the energy bands for Bloch waves were discovered in the context of atomic Bloch-Zener oscillations in an optical cavity. This problem is modeled by the system of a linear Schrödinger equation for the atomic wave function and an evolution equation for the number of photons in the cavity [5]. The stationary Bloch waves satisfy the Schrödinger equation, where the nonlinear response is captured by the dependence of the coefficient in front of the periodic potential V from the integral of the squared wave function multiplied by V . Prasanna, Larson, and O'Dell [6] discovered loops in the energy bands of the Bloch waves, which occur in the interior of the Brillouin zone and may detach as new energy bands, in a sharp contrast from the energy bands for Bloch waves in the optically trapped Bose-Einstein condensates.

The comparison between these two examples calls for systematic analysis of the loop bifurcations in the energy bands of the Bloch waves in periodic potentials. We study the latter phenomenon here, in the context of the Gross-Pitaevskii equation (1).

Consider now stationary states satisfying the time-independent Gross-Pitaevskii equation,

$$-\psi''(x) + V(x)\psi + c|\psi|^2\psi = \mu\psi, \tag{2}$$

with eigenvalue μ. Physically μ is associated with the chemical potential. We consider Bloch waves, which are quasi-periodic solutions of (2). That is,

$$\psi(x) = e^{ikx}\phi(x), \qquad x \in \mathbb{R}, \tag{3}$$

where $\phi(x)$ is a 2π-periodic function and k is the Bloch wavenumber. Therefore,

$$\psi(x + 2\pi) = e^{2\pi ik + ikx}\phi(x + 2\pi) = e^{2\pi ik}\psi(x). \tag{4}$$

Due to the periodicity of the exponential term in (4) it is sufficient to consider k on the interval $[-\frac{1}{2}, \frac{1}{2}]$, called the Brillouin zone.

For $k = 0$, (4) simplifies to $\psi(x + 2\pi) = \psi(x)$, a 2π-periodic function. For $k = \pm\frac{1}{2}$, (4) gives us $\psi(x + 2\pi) = -\psi(x)$, a 2π-antiperiodic function or a 4π-periodic function. At either $k = 0$ or $k = \pm\frac{1}{2}$ the function ψ can be taken to be purely real because (2) admits a reduction to real-valued solutions and the boundary conditions in (4) are real valued. We can not generally take ψ purely real for $k \neq \{0, \pm\frac{1}{2}\}$, as the boundary conditions in (4) are not real-valued.

We are interested in the qualitative behaviour of these functions, ψ, for varying values of the parameter c, specifically the appearance of a new solution at some bifurcation value $c = c_*$. In particular this analysis will reveal to us the loop structure in the Bloch bands as seen in [3] and [4].

The report is organized as follows. Section 2 deals with the stationary real branch and demonstrates, for $k = \pm\frac{1}{2}$, the unique continuation of solutions from $c = 0$ to some small $c \neq 0$. Section 3 presents asymptotic and numerical results for continuations of Bloch waves with $k = 0$ and $k = \frac{1}{2}$ as well as the eigenvalues of the linear Schrödinger operators associated with linearization of the time-independent Gross-Pitaevskii equation. Section 4 contains the main result; analysis of the bifurcation of the stationary real branch which is revealed to be a pitchfork bifurcation. Section 5 establishes the stability of solutions around the pitchfork bifurcation. Section 6 concludes the report. Appendix A addresses the validity of the numerical methods.

2 Stationary Real Branch

Let us consider $k = \frac{1}{2}$. Take ψ satisfying (2) defined on the interval $[-\pi, \pi]$ subject to antiperiodic boundary conditions. The natural space for these functions is,

$$\mathcal{H}^2_{a.p.} := \{f \in \mathcal{H}^2([-\pi, \pi], \mathbb{R}) : f(-\pi) = -f(\pi), f'(-\pi) = -f'(\pi)\}, \tag{5}$$

where,

$$\mathcal{H}^2([a, b], \mathbb{R}) := \{f : [a, b] \to \mathbb{R}, \|f\|_{\mathcal{H}^2} < \infty\}, \tag{6}$$

and

$$\|f\|_{\mathcal{H}^2} := \left(\int_a^b [(f'')^2 + (f')^2 + f^2]dx\right)^{\frac{1}{2}}. \tag{7}$$

Here we recall that $\mathcal{H}^2([-\pi, \pi], \mathbb{R})$ is embedded in the space of continuously differentiable functions $\mathcal{C}^1([-\pi, \pi], \mathbb{R})$. We define the inner product and the induced norm in $L^2([-\pi, \pi], \mathbb{R})$ by standard expressions,

$$< f, g >_{L^2} := \frac{1}{2\pi}\int_{-\pi}^{\pi} f(x)g(x)dx, \quad \|f\|^2_{L^2} :=< f, f >_{L^2} . \tag{8}$$

where $\frac{1}{2\pi}$ is included for convenience of normalization.

The linear analogue of (2), $c = 0$, in the space (5), exhibits well studied properties including the existence of a countable set of eigenvalues $\{\mu_n\}_{n\in\mathbb{N}_0}$, where $\mathbb{N}_0 := \{0, 1, 2, \ldots\}$, at discrete energy levels, each with a corresponding wave function, $\psi_n \in \mathcal{H}^2_{a.p.}$. We take each ψ_n to be real and normalized by $\|\psi_n\|_{L^2} = 1$. The main result of this section is formulated as follows.

Theorem 1. *Fix $n \in \mathbb{N}_0$. There exists $c_n > 0$ such that for any $c \in (-c_n, c_n)$, the stationary Gross-Pitaevskii equation,*

$$\begin{cases} -\psi'' + V(x)\psi + c\psi^3 = \mu\psi, & x \in \mathbb{R} \\ \psi(x + 2\pi) = -\psi(x), & x \in \mathbb{R} \\ \|\psi\|_{L^2} = 1 \end{cases} \tag{9}$$

admits a unique branch of solutions such that

$$|\mu - \mu_n| \leq D_1 c, \quad \|\psi - \psi_n\|_{\mathcal{H}^2} \leq D_2 c,$$

for some D_1, $D_2 > 0$.

The proof of the main theorem appears at the end of the section.

2.1 Preliminaries

We assume the existence of some $\psi_n \in \mathcal{H}^2_{a.p.}$ and μ_n satisfying (2) with $c = 0$. We also assume that $\mu_m \neq \mu_n$ for all $m \in \mathbb{N}_0 \backslash \{n\}$. Therefore, $L_n \psi_n = 0$ where,

$$L_n := -\partial_x^2 + V(x) - \mu_n, \tag{10}$$

is an unbounded operator from $\mathcal{H}^2_{a.p.}$ to L^2 which has a one-dimensional kernel in $\mathcal{H}^2_{a.p.}$, given by $\mathrm{Ker}(L_n) = \{\psi_n\}$. Since L_n is self-adjoint, its kernel and range are orthogonal so,

$$\mathrm{Ran}(L_n) = \{f \in L^2 : \ < f, \psi_n >_{L^2} = 0\}. \tag{11}$$

Therefore it is natural to introduce the decomposition, $L^2 = \{\psi_n\} \oplus \mathrm{Ran}(L_n)$ and define the projection operator, $P_n : L^2 \to \mathrm{Ran}(L_n)$. The norm $\|P_n L_n^{-1} P_n\|_{\mathcal{H}^2 \to \mathcal{H}^2}$ will become important for us shortly.

Lemma 1. *There exists $N > 0$ such that $\|P_n L_n^{-1} P_n\|_{\mathcal{H}^2 \to \mathcal{H}^2} \leq N$.*

Proof. The norm $\|P_n L_n^{-1} P_n\|_{\mathcal{H}^2 \to \mathcal{H}^2}$ is equivalent to the norm $\|P_n L_n^{-1} P_n\|_{L^2 \to L^2}$ defined by,

$$\|P_n L_n^{-1} P_n\|_{L^2 \to L^2} = \sup_{f \in L^2, f \neq 0} \frac{\|P_n L_n^{-1} P_n f\|_{L^2}}{\|f\|_{L^2}}. \tag{12}$$

Operator L_n is self-adjoint and so has an orthonormal set of eigenfunctions, $\{\psi_m\}_{m \in \mathbb{N}_0}$, that span L^2, for the set of eigenvalues $\{\mu_m - \mu_n\}_{m \in \mathbb{N}_0}$. Given $f \in L^2$ we can decompose f as,

$$f = \sum_{m \in \mathbb{N}_0} f_m \psi_m,$$

where, $f_m = < \psi_m, f >_{L^2}$. So,

$$\|f\|_{L^2}^2 = \sum_{m \in \mathbb{N}_0} \sum_{n \in \mathbb{N}_0} f_m f_n < \psi_m, \psi_n >_{L^2} = \sum_{m \in \mathbb{N}_0} f_m^2,$$

since $< \psi_m, \psi_n >_{L^2} = \delta_{m,n}$. The projection operator P_n simply kills the component of f in the direction of ψ_n. So,

$$P_n f = \sum_{m \in \mathbb{N}_0 \setminus \{n\}} f_m \psi_m$$

$$L_n^{-1} P_n f = \sum_{m \in \mathbb{N}_0 \setminus \{n\}} f_m L_n^{-1} \psi_m = \sum_{m \in \mathbb{N}_0 \setminus \{n\}} \frac{1}{\mu_m - \mu_n} f_m \psi_m + C\psi_0,$$

for any $C \in \mathbb{R}$. Applying P_n once more gives us,

$$P_n L_n^{-1} P_n f = \sum_{m \in \mathbb{N}_0 \setminus \{n\}} \frac{1}{\mu_m - \mu_n} f_m \varphi_m.$$

Taking the norm yields,

$$\begin{aligned} \|P_n L_n^{-1} P_n f\|_{L^2}^2 &= \sum_{m \in \mathbb{N}_0 \setminus \{n\}} \sum_{l \in \mathbb{N}_0 \setminus \{n\}} \frac{1}{(\mu_m - \mu_n)(\mu_l - \mu_n)} f_m f_l < \psi_m, \psi_l >_{L^2} = \sum_{m \in \mathbb{N}_0 \setminus \{n\}} \frac{f_m^2}{(\mu_m - \mu_n)^2} \\ &\leq \sup_{m \in \mathbb{N}_0 \setminus \{n\}} \frac{1}{|\mu_m - \mu_n|^2} \|f\|_{L^2}^2, \end{aligned}$$

so that,

$$\|P_n L_n^{-1} P_n\|_{L^2 \to L^2} = \sup_{m \in \mathbb{N}_0 \setminus \{n\}} \frac{1}{|\mu_m - \mu_n|} = \left(\inf_{m \in \mathbb{N}_0 \setminus \{n\}} |\mu_m - \mu_n| \right)^{-1}.$$

□

We will also use the following property of $\mathcal{H}^2$: for any f, $g \in \mathcal{H}^2$, there is $K > 0$ such that,

$$\|fg\|_{\mathcal{H}^2} \leq K \|f\|_{\mathcal{H}^2} \|g\|_{\mathcal{H}^2}. \tag{13}$$

This property shows that $\mathcal{H}^2$ is a Banach Algebra with respect to pointwise multiplication.

2.2 Lyapunov-Schmidt Reduction

Now take $c > 0$ and consider a solution of (9), ψ with nonlinear eigenvalue μ. Decompose μ into $\mu = \mu_n + \delta\mu$. Let us write (9) in the equivalent form,

$$L_n \psi = \delta\mu\psi - c\psi^3 \equiv \mathcal{F}. \tag{14}$$

$\mathcal{F}$ must be in the range of L_n, so it follows that,

$$< \delta\mu\psi - c\psi^3, \psi_n >_{L^2} = 0 \quad \Rightarrow \quad \delta\mu = c \frac{< \psi^3, \psi_n >_{L^2}}{< \psi, \psi_n >_{L^2}}. \tag{15}$$

Decompose ψ as $\psi = a\psi_n + \delta\psi$, with $a \in \mathbb{R}$, and $< \psi_n, \delta\psi >_{L^2} = 0$. Then (15) yields, at the leading order,

$$\delta\mu = \frac{c}{a} < (a\psi_n + \delta\psi)^3, \psi_n >_{L^2} \equiv f(\delta\psi, c), \tag{16}$$

so that,

$$\delta\mu = c(a^2\|\psi_n\|_{L^4}^4 + \mathcal{O}(a\|\delta\psi\|_{\mathcal{H}^2})), \tag{17}$$

provided $\|\delta\psi\|_{\mathcal{H}} \ll |a|$. The normalization of ψ and ψ_n gives,

$$1 = a^2 + \|\delta\psi\|_{L^2}^2 \quad \Rightarrow \quad a = \sqrt{1 - \|\delta\psi\|_{L^2}^2} \equiv g(\delta\psi), \tag{18}$$

So,

$$a = 1 + \mathcal{O}(\|\delta\psi\|_{\mathcal{H}^2}^2), \tag{19}$$

and,

$$\delta\mu = c(\|\psi_n\|_{L^4}^4 + \mathcal{O}(\|\delta\psi\|_{\mathcal{H}^2})). \tag{20}$$

We now turn our attention to $\delta\psi$. Note that since $\psi_n \in \mathrm{Ker}(L_n)$ we have,

$$\mathcal{F} = L_n\psi = L_n(\psi_n + \delta\psi) = L_n\delta\psi. \tag{21}$$

Then,

$$\begin{aligned} \delta\psi &= (P_nL_n^{-1}P_n)\mathcal{F} \\ &= (P_nL_n^{-1}P_n)(\delta\mu(a\psi_n + \delta\psi) - c(a\psi_n + \delta\psi)^3) \\ &\equiv \mathcal{A}(\delta\psi; c). \end{aligned} \tag{22}$$

The nonlinear operator $\mathcal{A}$ depends only on $\delta\psi \in \mathcal{H}^2_{a.p.}$ and $c \in \mathbb{R}$ since $\delta\mu$ and a are uniquely determined by constraint (16) and normalization (18).

Lemma 2. *There is $c_n > 0$ such that for any $c \in (-c_n, c_n)$, $\mathcal{A}(\delta\psi; c)$, as defined by* (16), (18) *and* (22), *has a unique fixed point, $\delta\psi \in \mathcal{H}^2_{a.p.}$, in a neighbourhood of $0 \in \mathcal{H}^2_{a.p.}$. Moreover, there exists $D > 0$ such that $\|\delta\psi\|_{\mathcal{H}^2} \leq Dc$.*

Proof. We will apply the Banach Fixed Point Theorem (see Section 1.6 in [1] for a precise statement) to the proof of existence and uniqueness of a fixed point of $\mathcal{A}$. We must show that $\mathcal{A}$ maps a closed neighbourhood around $0 \in \mathcal{H}^2_{a.p.}$ into itself and that $\mathcal{A}$ is a contraction map. Take $\bar{\mathcal{B}}_\varepsilon \subset \mathcal{H}^2_{a.p.}$ with,

$$\bar{\mathcal{B}}_\varepsilon := \{\psi \in \mathcal{H}^2_{a.p.} : \|\psi\|_{\mathcal{H}^2} \leq \varepsilon\}, \tag{23}$$

a closed neighbourhood around $0 \in \mathcal{H}^2_{a.p.}$. Take $\delta\psi \in \bar{\mathcal{B}}_\varepsilon$ and consider the norm of $\mathcal{A}(\delta\psi; c)$ for small c. Note that $\psi_n \in \mathcal{H}^2$ gives $\|\psi_n\|_{\mathcal{H}^2} \leq R$ for some $R > 0$, Lemma 1 gives $\|P_nL_n^{-1}P_n\|_{\mathcal{H}^2 \to \mathcal{H}^2} \leq N$ and recall the property (13) with $\|fg\|_{\mathcal{H}^2} \leq K\|f\|_{\mathcal{H}^2}\|g\|_{\mathcal{H}^2}$. Then we have,

$$\begin{aligned} \|\mathcal{A}(\delta\psi; c)\|_{\mathcal{H}^2} &= \|P_nL_n^{-1}P_n\|_{\mathcal{H}^2 \to \mathcal{H}^2}\|\delta\mu(a\psi_n + \delta\psi) - c(a\psi_n + \delta\psi)^3\|_{\mathcal{H}^2} \\ &\leq N(R|a||\delta\mu| + |\delta\mu|\varepsilon + cK^2(R^3|a|^3 + 3R^2|a|^2\varepsilon + 3R|a|\varepsilon^2 + \varepsilon^3)). \end{aligned} \tag{24}$$

Since $|\delta\mu| = \mathcal{O}(c)$ from (20) if $\delta\psi \in \bar{\mathcal{B}}_\varepsilon$, there is a $c_n > 0$ such that for all $c \in (-c_n, c_n)$, there is $\varepsilon = \varepsilon(c)$ such that $\|\mathcal{A}(\delta\psi; c)\|_{\mathcal{H}^2} \leq \varepsilon$ if $\|\delta\psi\|_{\mathcal{H}^2} \leq \varepsilon$. Hence $\mathcal{A}$ maps a closed ball in $\mathcal{H}^2_{a.p.}$ into itself.

Now we show that $\mathcal{A}$ is a contraction map for small c. That is, we need to show that there is $c_n > 0$ such that for all $c \in (-c_n, c_n)$ there is $q = q(c)$ such that $q \in (0,1)$ and,

$$\|\mathcal{A}(\delta\psi_1; c) - \mathcal{A}(\delta\psi_2; c)\|_{\mathcal{H}^2} \leq q\|\delta\psi_1 - \delta\psi_2\|_{\mathcal{H}^2}, \tag{25}$$

where,

$$\begin{aligned}\mathcal{A}(\delta\psi_1; c) - \mathcal{A}(\delta\psi_2; c) = P_n L_n^{-1} P_n((\delta\mu_1 a_1 - \delta\mu_2 a_2)\psi_n + \delta\mu_1\delta\psi_1 - \delta\mu_2\delta\psi_2 - c((a_1^3 - a_2^3)\psi_n^3 \\ + 3\psi_n^2(a_1^2\delta\psi_1 - a_2^2\delta\psi_2) + 3\psi_n(a_1\delta\psi_1^2 - a_2\delta\psi_2^2) + (\delta\psi_1^3 - \delta\psi_2^3))).\end{aligned} \tag{26}$$

Note that $\delta\mu = f(\delta\psi, c)$ in (16) depends only on c and $\delta\psi$ since we have determined $a = g(\delta\psi)$ from (18). We also recall $\delta\psi_1$, $\delta\psi_2 \in \bar{\mathcal{B}}_\varepsilon$ and all bounds used previously. We now treat some terms in (26). Firstly,

$$\begin{aligned}\|(\delta\mu_1 a_1 - \delta\mu_2 a_2)\psi_n\|_{\mathcal{H}^2} &\leq |\delta\mu_1 a_1 - \delta\mu_2 a_2|\|\psi_n\|_{\mathcal{H}^2} \\ &\leq M_1|c|\|\delta\psi_1 - \delta\psi_2\|_{\mathcal{H}^2},\end{aligned} \tag{27}$$

for some $M_1 > 0$ using (19) and (20). Secondly,

$$\begin{aligned}\|\delta\mu_1\delta\psi_1 - \delta\mu_2\delta\psi_2\|_{\mathcal{H}^2} &\leq \|\delta\mu_1(\delta\psi_1 - \delta\psi_2)\|_{\mathcal{H}^2} + \|(\delta\mu_1 - \delta\mu_2)\delta\psi_2\|_{\mathcal{H}^2} \\ &\leq M_2\varepsilon|c|\|\delta\psi_1 - \delta\psi_2\|_{\mathcal{H}^2},\end{aligned} \tag{28}$$

for some $M_2 > 0$, again with the help of (20). Thirdly,

$$\begin{aligned}\|(a_1^3 - a_2^3)\psi_n^3\|_{\mathcal{H}^2} &\leq K^2|a_1^3 - a_2^3|\|\psi_n\|_{\mathcal{H}^2}^3 \\ &\leq K^2R^3|a_1 - a_2||a_1^2 + a_1a_2 + a_2^2| \\ &\leq K^3R^3\frac{|a_1^2 + a_1a_2 + a_2^2|}{|a_1 + a_2|}\|\delta\psi_1 - \delta\psi_2\|_{\mathcal{H}^2}\|\delta\psi_1 + \delta\psi_2\|_{\mathcal{H}^2} \\ &\leq M_3\varepsilon\|\delta\psi_1 - \delta\psi_2\|_{\mathcal{H}^2},\end{aligned} \tag{29}$$

for some $M_3 > 0$ with the application of (19). Fourthly,

$$\begin{aligned}\|\delta\psi_1^3 - \delta\psi_2^3\|_{\mathcal{H}^2} &\leq K\|\delta\psi_1 - \delta\psi_2\|_{\mathcal{H}^2}\|\delta\psi_1^2 + \delta\psi_1\delta\psi_2 + \delta\psi_2^2\|_{\mathcal{H}^2} \\ &\leq M_4\varepsilon^2\|\delta\psi_1 - \delta\psi_2\|_{\mathcal{H}^2},\end{aligned} \tag{30}$$

for some $M_4 > 0$. Finally, the other two terms can be estimated similarly to (29) − (30) and are bounded as follows,

$$\|3\psi_n^2(a_1^2\delta\psi_1 - a_2^2\delta\psi_2)\|_{\mathcal{H}^2} \leq M_5\|\delta\psi_1 - \delta\psi_2\|_{\mathcal{H}^2}, \tag{31}$$

$$\|3\psi_n(a_1\delta\psi_1^2 - a_2\delta\psi_2^2)\|_{\mathcal{H}^2} \leq M_6\varepsilon\|\delta\psi_1 - \delta\psi_2\|_{\mathcal{H}^2}, \tag{32}$$

for some $M_5 > 0$ and $M_6 > 0$. Putting everything together yields (25) with,

$$q := |c|N(M_1 + M_5 + (M_2 + M_3 + M_6)\varepsilon + M_4\varepsilon^2). \tag{33}$$

It is clear that there exists $c_n > 0$ such that $q < 1$ for all $c \in (-c_n, c_n)$ and so $\mathcal{A}$ is a contraction mapping. Thus, by the Banach Fixed Point Theorem [1], we have the existence of a unique fixed point, $\delta\psi \in \mathcal{H}^2_{a.p.}$, of $\mathcal{A}$ for sufficiently small c.

Now, let us make an estimate on the order of $\delta\psi$ for small c. Expansion of (19), (20) and (22) gives, at the leading order,

$$\delta\psi = c(P_n L_n^{-1} P_n)(\|\psi_n\|_{L^4}^4 \psi_n - \psi_n^3 + \mathcal{O}(\|\delta\psi\|_{\mathcal{H}^2})). \tag{34}$$

Hence, (34) gives for the unique fixed point $\delta\psi \in \mathcal{H}^2_{a.p.}$,

$$\delta\psi = c(P_n L_n^{-1} P_n)(\|\psi_n\|_{L^4}^4 \psi_n - \psi_n^3) + \mathcal{O}(c^2), \tag{35}$$

so that there is $D > 0$ such that $\|\delta\psi\|_{\mathcal{H}^2} \leq Dc$. □

We now prove the main theorem.

Proof of Theorem 1. From (19), (20) and Lemma 2 we have uniquely determined $\delta\psi$ and $\delta\mu$ and thus, ψ and μ where,

$$\psi = a\psi_n + \delta\psi, \qquad \mu = \mu_n + \delta\mu,$$

with,

$$\|\delta\psi\|_{\mathcal{H}^2} = \mathcal{O}(c), \qquad |\delta\mu| = \mathcal{O}(c), \qquad |a-1| = \mathcal{O}(c^2).$$

Hence, $|\mu - \mu_n| \leq D_1 c$ and $\|\psi - \psi_n\|_{\mathcal{H}^2} \leq D_2 c$ for some D_1, $D_2 > 0$, as required. □

We refer to this unique continuation as the stationary real branch. Note that the above argument applies equally well for periodic boundary conditions in (9), that is for, $k = 0$ with $\psi \in \mathcal{H}^2_{per}$ where,

$$\mathcal{H}^2_{per} := \{f \in \mathcal{H}^2([-\pi, \pi], \mathbb{R}) : f(-\pi) = f(\pi), f'(-\pi) = f'(\pi)\}. \tag{36}$$

In fact, a more careful treatment of the above yields a unique continuation in c of Bloch waves for all $k \in [-\frac{1}{2}, \frac{1}{2}]$. Of course the result only holds in a neighbourhood of small c. A further increase in c may lead to a change in the number of solutions of the stationary equation (2).

3 Perturbative and Numerical Results

Before we start to analyse solutions along the stationary real branch and look for bifurcations we must first introduce the following linearization operators,

$$L_+ := -\partial_x^2 + V(x) + 3c\psi^2(x) - \mu, \tag{37}$$
$$L_- := -\partial_x^2 + V(x) + c\psi^2(x) - \mu, \tag{38}$$

where ψ is a stationary real solution of (2) corresponding to the nonlinear eigenvalue μ. L_+ can be obtained by differentiating (2) with respect to real ψ. Differentiating (2) with respect to imaginary ψ yields L_-. It is necessary to note that $L_-\psi = 0$ if ψ satisfies (2). Since we are interested in bifurcations of stationary solutions, we examine the eigenvalues of $L_\pm$ and look for a change in the number of zero eigenvalues.

3.1 Asymptotic Approximations

In this section we obtain linear approximations of eigenvalues of $L_\pm$ at $c = 0$. Let us consider $\mu(c)$ along the branch of real-valued solutions ψ originating from the linear eigenmode ψ_n, as described in Section 2. The dependence of μ from c comes from $\delta\mu$ as in (20). So,

$$\left.\frac{d\mu}{dc}\right|_{c=0} = \lim_{c\to 0}\frac{\mu-\mu_n}{c} = \lim_{c\to 0}\frac{\delta\mu}{c} = \|\psi_n\|_{L^4}^4. \tag{39}$$

Now consider $L_\pm$ and their eigenvalues along the branch $\mu(c)$. Denote the eigenvalues of $L_\pm$ by $\lambda_\pm^{(m)}$, $m \in \mathbb{N}_0$ and their L^2 normalized eigenfunctions $\varphi_\pm^{(m)}$. The Rayleigh quotient gives,

$$\lambda_\pm^{(m)}(c) =< L_\pm(c)\varphi_\pm^{(m)}, \varphi_\pm^{(m)} >_{L^2} . \tag{40}$$

We note that $L_+(0) = L_-(0) = -\partial_x^2 + V(x) - \mu_n \equiv L_n$, which has eigenvalues $\lambda_\pm^{(m)} = \mu_m - \mu_n$ with normalized eigenfunctions $\varphi_\pm^{(m)}\big|_{c=0} = \psi_m$. We also note that,

$$L_+'(0) = 3\psi^2\Big|_{c=0} - \mu'(0) = 3\psi_n^2 - \|\psi_n\|_{L^4}^4, \tag{41}$$

$$L_-'(0) = \psi^2\Big|_{c=0} - \mu'(0) = \psi_n^2 - \|\psi_n\|_{L^4}^4. \tag{42}$$

Therefore,

$$\left.\frac{d\lambda_-^{(m)}}{dc}\right|_{c=0} =< L_-'(0)\psi_m, \psi_m >_{L^2} =< \psi_n^2, \psi_m^2 >_{L^2} -\|\psi_n\|_{L^4}^4. \tag{43}$$

Similarly,

$$\left.\frac{d\lambda_+^{(m)}}{dc}\right|_{c=0} = 3 < \psi_n^2, \psi_m^2 >_{L^2} -\|\psi_n\|_{L^4}^4. \tag{44}$$

At $c = 0$, $L_\pm(0) = L_n$ has a simple zero eigenvalue and n negative eigenvalues. The rest of the purely discrete spectrum of $L_\pm(0)$ is strictly positive. Since,

$$\left.\frac{d\lambda_+^{(n)}}{dc}\right|_{c=0} = 2\|\psi_n\|_{L^4}^4 > 0, \tag{45}$$

operator L_+ has n negative and no zero eigenvalues for small $c > 0$ and $(n + 1)$ negative and no zero eigenvalues for $c < 0$. Operator L_- has n negative and one zero eigenvalue for small $c \neq 0$. Indeed,

$$\left.\frac{d\lambda_-^{(n)}}{dc}\right|_{c=0} = 0, \tag{46}$$

and we recall that $L_-(c)\psi = 0$.

We now prove for $c > 0$ that the number of negative eigenvalues of $L_+(c)$ cannot exceed the number of negative eigenvalues of $L_-(c)$.

Lemma 3. *Suppose that the spectrum of L_- has κ negative eigenvalues and a simple zero eigenvalue. Then for $c > 0$ the spectrum of L_+ has at most κ negative and zero eigenvalues with the account of their multiplicity.*

Proof. It is clear from (37) and (38) that

$$L_+ = L_- + 2c\psi^2(x).$$

Note that since L_+ and L_- are self-adjoint, their eigenfunctions form an orthogonal basis for $\mathcal{H}^2_{a.p.}$. Denote the negative and zero eigenvalues of L_- by,

$$L_- u_n = \lambda_n u_n, \quad 0 \le n \le \kappa, \tag{47}$$

where, $\lambda_0 = 0 > \lambda_1 \ge \ldots \ge \lambda_k$ including eigenvalues with multiplicity greater than one. Similarly, for L_+ write,

$$L_+ w_n = \gamma_n w_n, \quad 1 \le n \le m, \tag{48}$$

where, $\gamma_m \le \gamma_{m-1} \le \ldots \le \gamma_1 \le 0$. We claim that $m \le \kappa$. Suppose $m > \kappa$ and derive a contradiction. For $f \in \text{span}\{w_1, \ldots w_m\}$, we write,

$$f = \sum_{n=1}^{m} c_n w_n, \tag{49}$$

for coefficients c_n and note that,

$$< L_+ f, f >_{L^2} = \sum_{n=1}^{m} |c_n|^2 \gamma_n \le 0, \tag{50}$$

because of the orthogonality of w_n. Now let us write w_n as an orthogonal decomposition over eigenfunctions of L_-,

$$w_n = \sum_{l=1}^{\kappa} a_{n,l} u_l + \widetilde{w}_n, \quad \widetilde{w}_n \perp \text{span}\{u_1, \ldots, u_\kappa\}, \tag{51}$$

with $< L_- \widetilde{w}_n, \widetilde{w}_n >_{L^2} \ge 0$. Consider,

$$g = \sum_{n=1}^{m} b_n w_n + \widetilde{g} = \sum_{l=1}^{\kappa} \left(\sum_{n=1}^{m} a_{n,l} b_n \right) u_l + \widetilde{g} + \sum_{n=1}^{m} b_n \widetilde{w}_n, \tag{52}$$

with, $\widetilde{g} \perp \text{span}\{u_1, \ldots, u_\kappa\}$ and upon substituting our decomposition for w_n. In particular, if $g = 0$ then, (52) represents a decomposition of 0 over eigenfunctions of L_-, so that,

$$\widetilde{g} = -\sum_{n=1}^{m} b_n \widetilde{w}_n = -\sum_{n=1}^{m} b_n w_n, \tag{53}$$

and,

$$\sum_{n=1}^{m} a_{n,l} b_n = 0, \quad 1 \le l \le \kappa. \tag{54}$$

If $m > \kappa$ then there exists a non-zero solution for $\{b_1, \ldots, b_m\}$ in the under-determined linear system (54). So $\widetilde{g}$ in (53) is a non-zero vector. Since $\widetilde{g} \in \text{span}\{w_1, \ldots, w_m\}$, (50) gives,

$$< L_+\widetilde{g}, \widetilde{g} >_{L^2} = \sum_{n=1}^{m} |b_n|^2 \gamma_m \leq 0. \tag{55}$$

On the other hand, since $\widetilde{g} \in \text{span}\{\widetilde{w}_1, \ldots, \widetilde{w}_m\} \perp \text{span}\{u_1, \ldots, u_\kappa\}$ and $\widetilde{g} \neq 0$, we have $< L_-\widetilde{g}, \widetilde{g} >_{L^2} \geq 0$ and,

$$< L_+\widetilde{g}, \widetilde{g} >_{L^2} = < L_-\widetilde{g}, \widetilde{g} >_{L^2} + 2c < \psi^2, \widetilde{g}^2 >_{L^2} > 0. \tag{56}$$

This gives the desired contradiction and so we conclude that $m \leq \kappa$. □

Corollary 1. *Assume that $\kappa = 0$. Then, as $c > 0$ increases, L_- acquires an additional zero eigenvalue before L_+ acquires a first zero eigenvalue.*

Corollary 1 is applied to the lowest energy band, for which $\kappa = 0$ at least for small values of c.

3.2 Numerical Results

We would like to construct numerical approximations of the real Bloch waves (for $k = 0$ and $k = \frac{1}{2}$) as well as eigenvalues of the operators L_+ and L_-. Numerically we solve the second-order differential equation,

$$-\phi''(x) + V(x)\phi \pm \phi^3 = \mu\phi, \quad x \in [-\pi, \pi] \tag{57}$$

with continuous parameter μ. We solve (57) using a shooting method by taking advantage of the boundary conditions: $\phi(x + 2\pi) = -\phi(x)$ for $k = \frac{1}{2}$ or $\phi(x + 2\pi) = \phi(x)$ for $k = 0$. Once we have ϕ for a given value of μ, we compute c and ψ in the stationary Gross-Pitaevskii equation (2) by,

$$\psi = \frac{1}{\sqrt{N}}\phi, \quad c = \pm N, \tag{58}$$

where $N = \|\phi\|_{L^2}^2$. Once we have determined c and ψ we have operators $L_\pm$ and can numerically approximate their eigenvalues. In the figures that follow we use $V(x) = \cos(x)$ as the potential. Note that in Figure 1(c) the bifurcation at $c = 1$ is exactly the loop bifurcation mentioned in [3].

The most interesting aspect of Figures 1-6 are the values of c for which the number of negative eigenvalues of L_- changes. This phenomenon is seen in Figure 1c (at $c = 1$), Figure 3c (around $c = 0.05$), and Figure 5c (around $c = 0.4$) for positive c and in 6c (around $c = -0.3$) for negative c.

No change in the number of negative eigenvalues is observed for operator L_+. The change in the number of negative eigenvalues of L_- leads to a bifurcation in the stationary real branch in the space of complex functions. We analyse this bifurcation in the next section.

4 Pitchfork Bifurcation along the Real Branch

Here we consider only $k = \frac{1}{2}$ for simplicity. Pick a real branch of stationary solutions $\psi(x; c)$, as in Theorem 1, for some fixed $n \in \mathbb{N}_0$. Recall that for small c, L_+ is invertible and L_- has a one

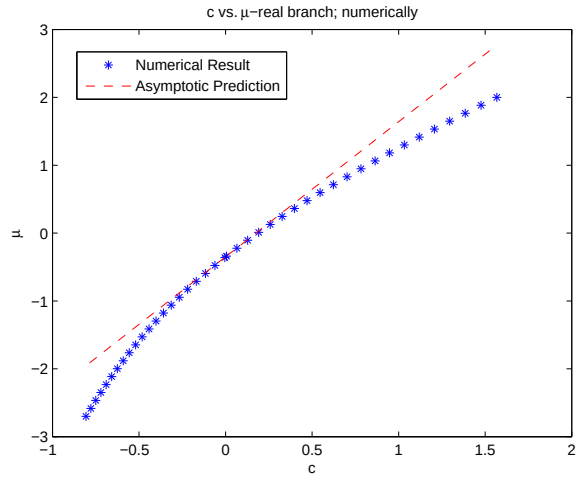

(a)

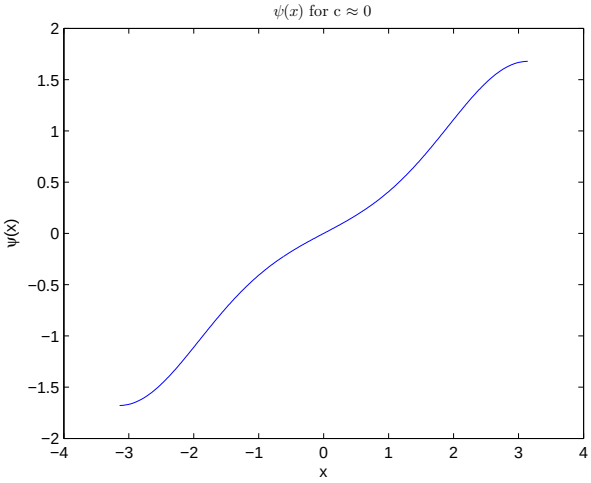

(b)

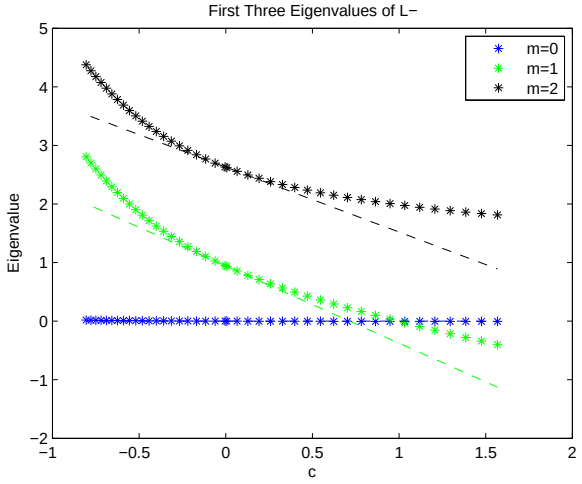

(c)

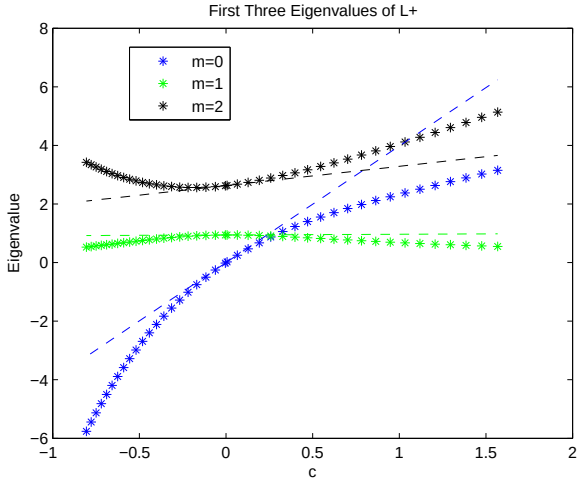

(d)

Figure 1: Numerical results for $k = \frac{1}{2}$ $n = 0$. Dashes lines denote linear approximations as calculated in section 3.1. Astrix give numerical results. (a) values μ for various c on the stationary real branch. (b) Wave function ψ close to $c = 0$. (c) Eigenvalues for L_-. Note the change in sign of eigenvalue $m = 1$ at $c = 1$. (d) Eigenvalues for L_+.

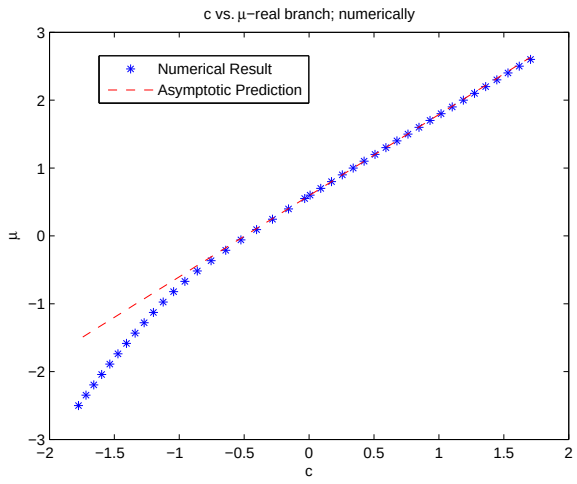

(a)

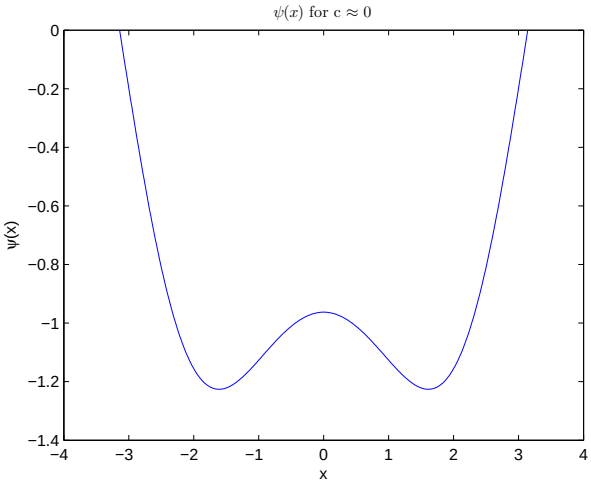

(b)

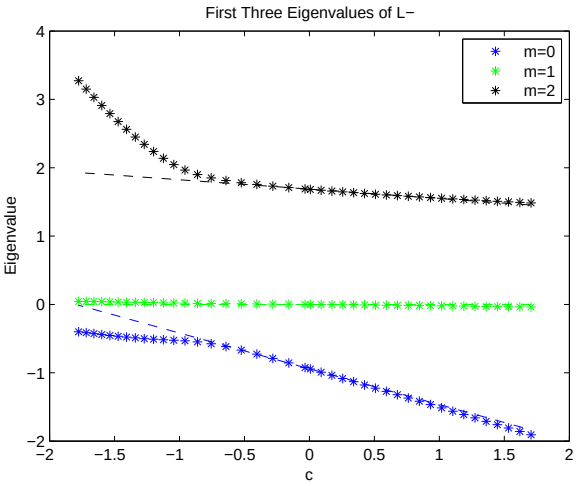

(c)

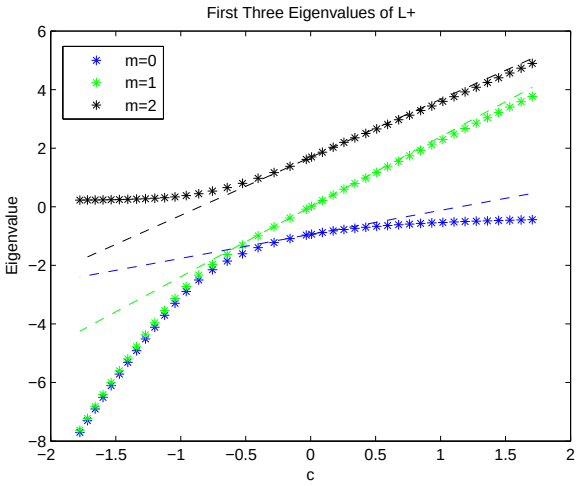

(d)

Figure 2: Similar to Figure 1 but with $k = \frac{1}{2}$ and $n = 1$.

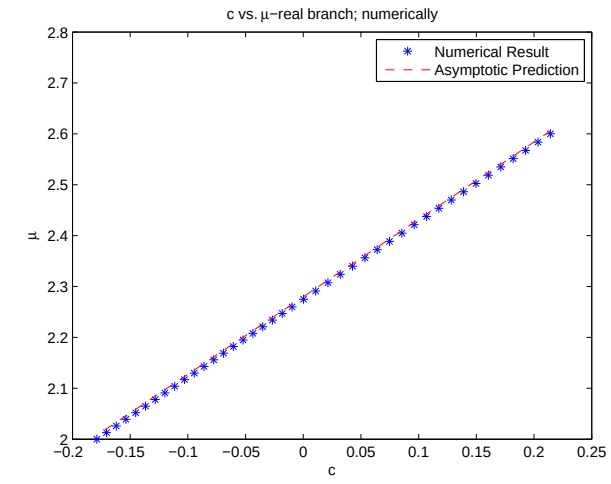

(a)

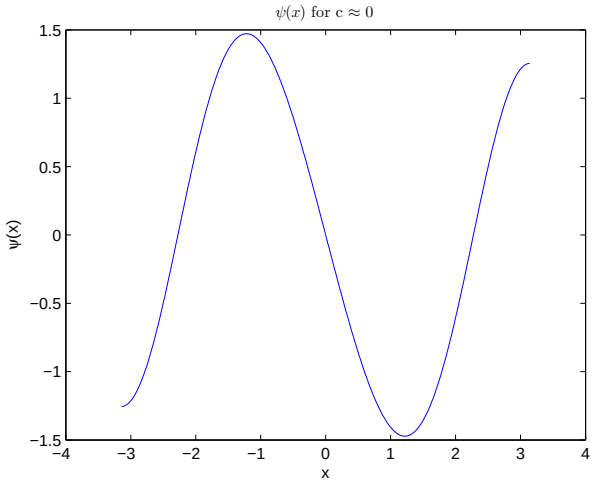

(b)

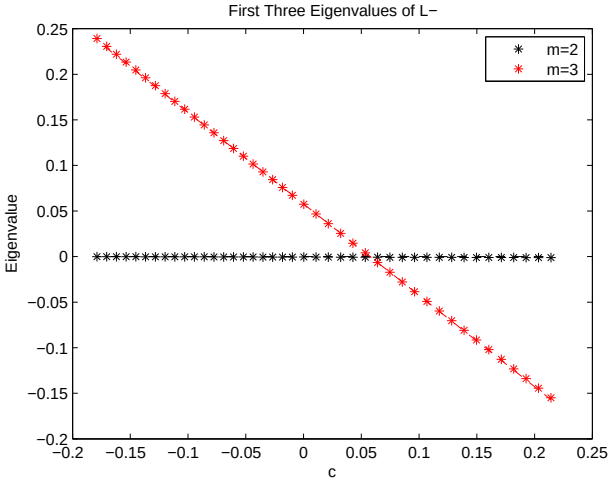

(c)

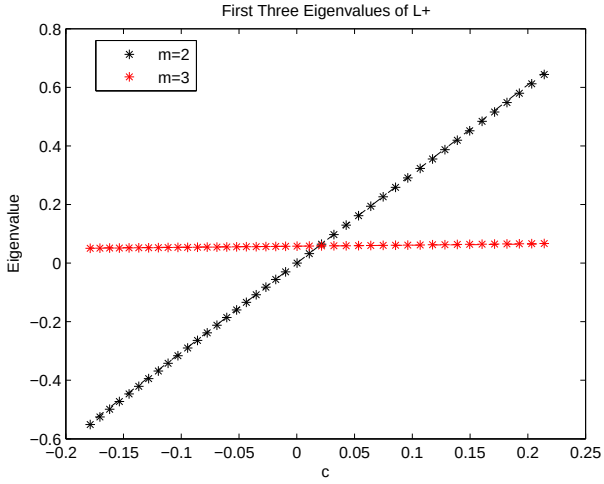

(d)

Figure 3: Similar to Figure 1 but with $k = \frac{1}{2}$ and $n = 2$. Note the change in sign of eigenvalue $m = 3$ of L_- at $c \approx 0.05$.

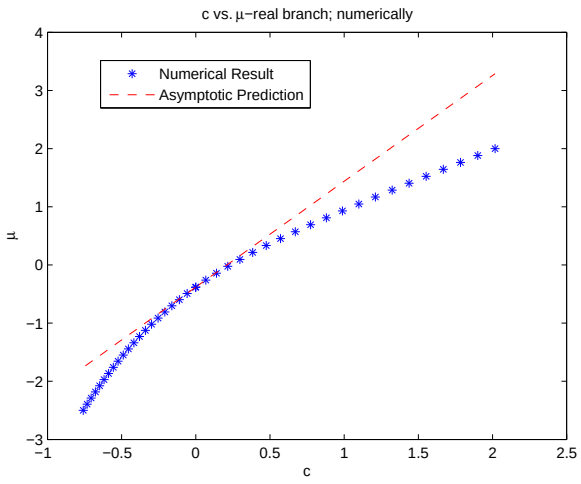

(a)

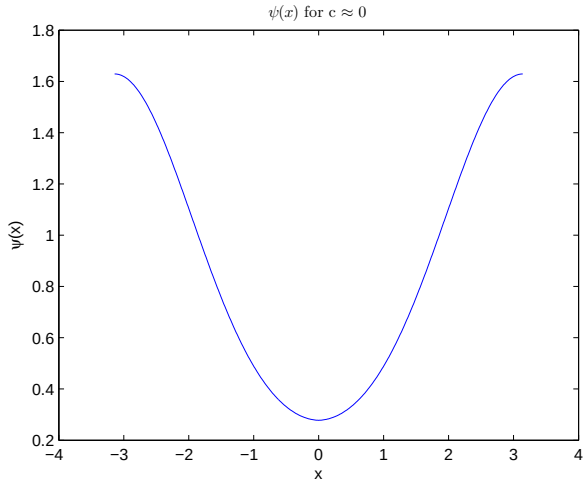

(b)

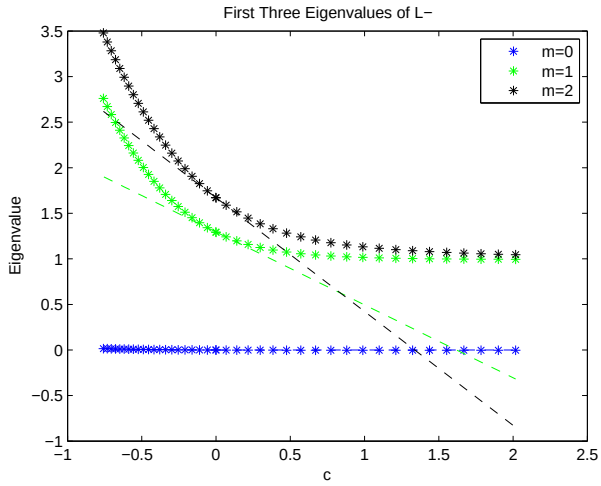

(c)

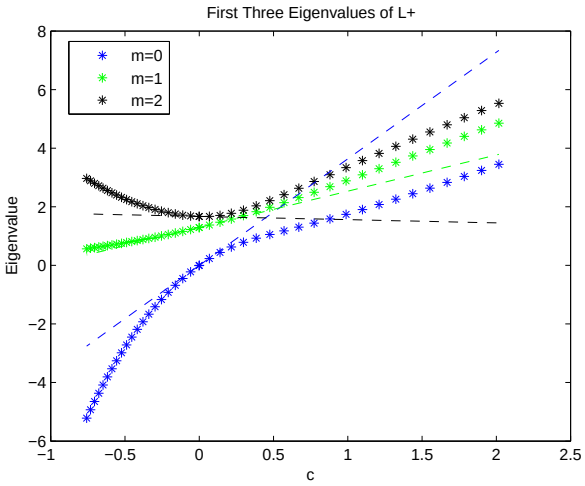

(d)

Figure 4: Similar to Figure 1 but with $k = 0$ and $n = 0$.

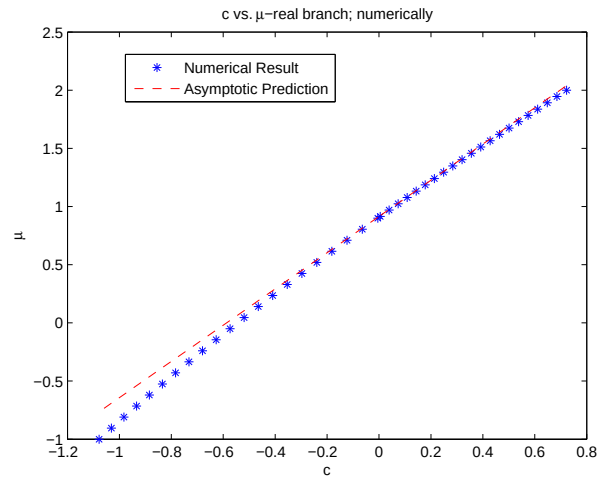

(a)

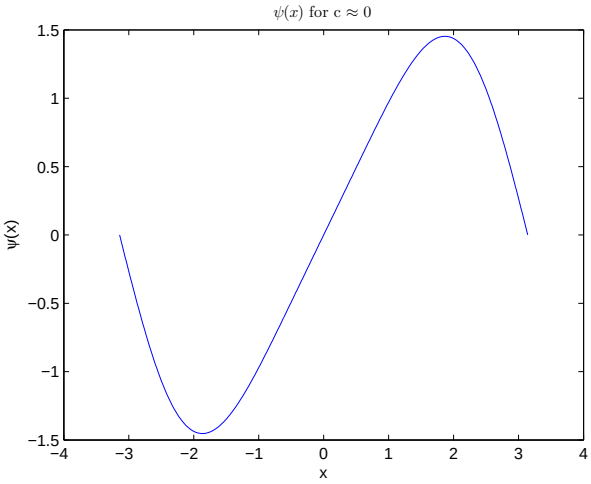

(b)

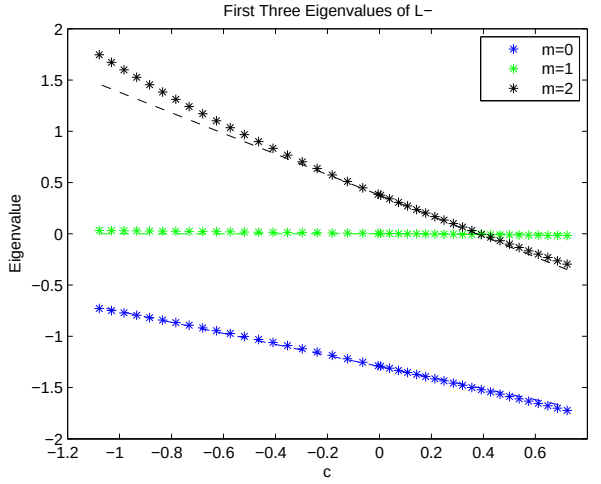

(c)

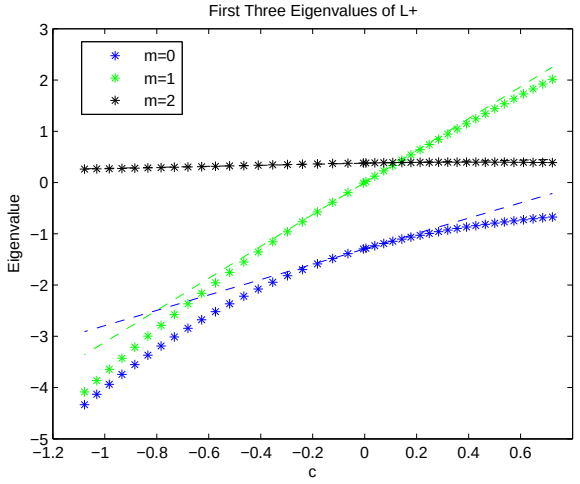

(d)

Figure 5: Similar to Figure 1 but with $k = 0$ and $n = 1$. Note the change in sign of eigenvalue $m = 2$ of L_- at $c \approx 0.4$.

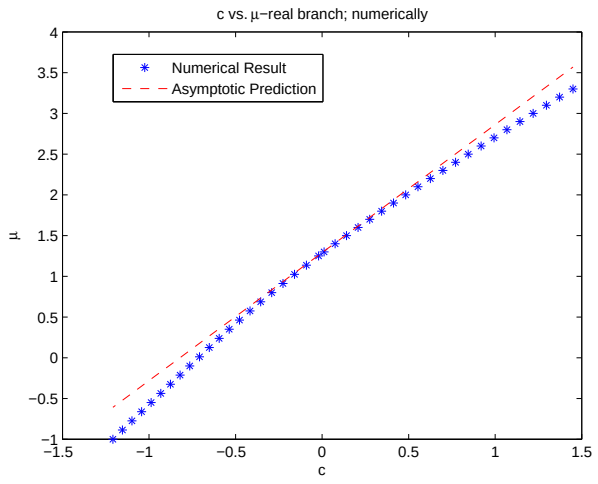

(a)

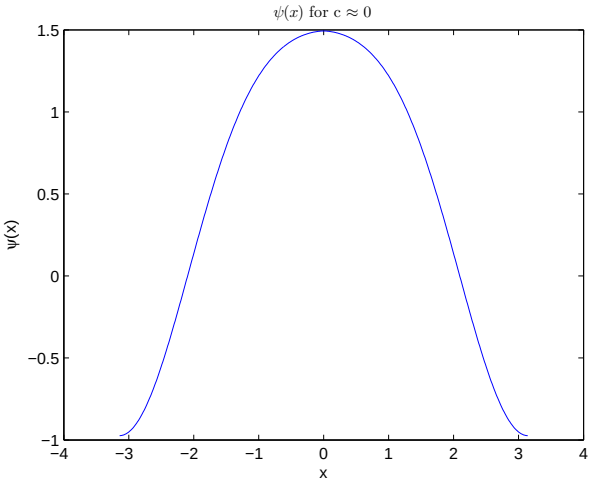

(b)

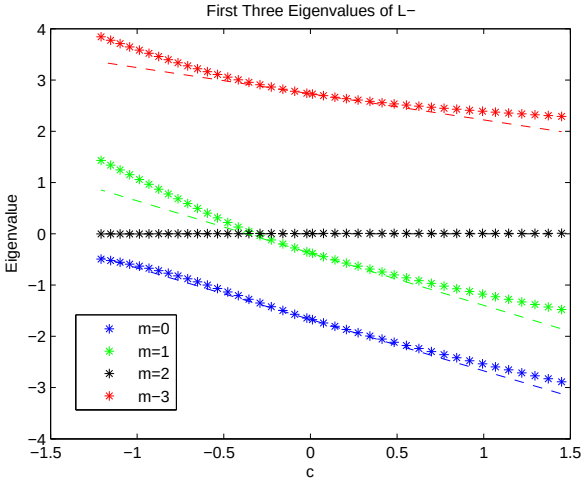

(c)

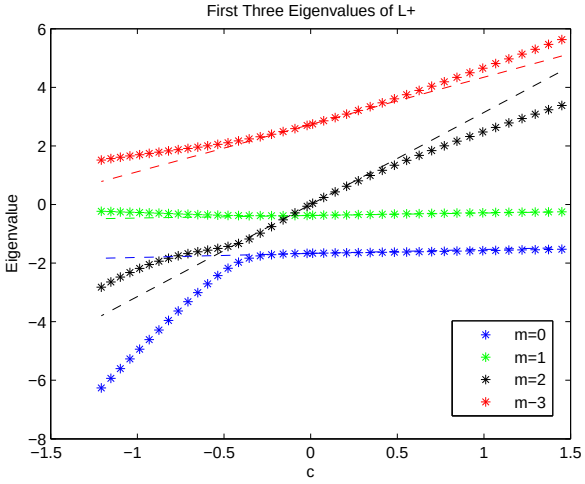

(d)

Figure 6: Similar to Figure 1 but with $k = 0$ and $n = 2$. Note the change in sign of eigenvalue $m = 1$ of L_- at $c \approx -0.3$.

dimensional kernel spanned by ψ_*. We assume that L_+ remains invertible for small values of c but the kernel of L_- becomes two dimensional for a particular value of c. Examples of this occur in Figure 1 and Figure 3 for $k = \frac{1}{2}$. Call this special value of c by c_*. Denote $\mu_* := \mu_n(c_*)$, $\psi_*(x) := \psi(x; c_*)$ and,

$$L_+^* := -\partial_x^2 + V(x) + 3c_*\psi_*^2(x) - \mu_*, \tag{59}$$
$$L_-^* := -\partial_x^2 + V(x) + c_*\psi_*^2(x) - \mu_*. \tag{60}$$

Recall that $L_-^*\psi_* = 0$. We then define the bifurcation at $c = c_*$ according to the following two conditions,

(A1) L_+^* is invertible

(A2) $\exists \varphi_* \in \mathcal{H}^2_{a.p.}$ such that $L_-^*\varphi_* = 0$ and $< \varphi_*, \psi_* >_{L^2} = 0$.

We now formulate the main theorem for this section. The proof appears at the end of the section.

Theorem 2. *Assume that* (A1) *and* (A2) *hold. Suppose that,*

$$S_0 \equiv < \psi_*, (L_+^*)^{-1}\psi_* >_{L^2} \neq 0$$
$$P_0 \equiv - < \psi_*^2, \varphi_*^2 >_{L^2} + 2c_* < \psi_*\varphi_*^2, (L_+^*)^{-1}\psi_*^3 >_{L^2} + \alpha_0(1 - 2c_* < \psi_*\varphi_*^2, (L_+^*)^{-1}\psi_* >_{L^2}) \neq 0,$$
$$Q_0 \equiv c_*(2c_* < \psi_*\varphi_*^2, (L_+^*)^{-1}\varphi_*^2\psi_* >_{L^2} - \|\varphi_*\|_{L^4}^4) + \beta_0(1 - 2c_* < \psi_*\varphi_*^2, (L_+^*)^{-1}\psi_* >_{L^2}) \neq 0,$$
$$R_0 \equiv 2 < \psi_*', \varphi_* >_{L^2} \neq 0,$$

where,

$$\alpha_0 \equiv \frac{< \psi_*, (L_+^*)^{-1}\psi_*^3 >_{L^2}}{< \psi_*, (L_+^*)^{-1}\psi_* >_{L^2}}, \quad \beta_0 \equiv \frac{2c_* < \psi_*, (L_+^*)^{-1}\varphi_*^2\psi_* >_{L^2} - 1}{2 < \psi_*, (L_+^*)^{-1}\psi_* >_{L^2}}.$$

If $\operatorname{sign}(P_0Q_0) = -1$*, there exists* $\varepsilon_0 > 0$*,* $\delta > 0$ *and* $\eta > 0$ *such that the stationary Gross-Pitaevskii equation* (2) *with* $c = c_* + \varepsilon$ *admits a unique Bloch wave solution* (4) *for all* $\varepsilon \in (-\varepsilon_0, 0]$ *and* $|k - \frac{1}{2}| < \delta$ *and three Bloch wave solutions* (4) *for all* $\varepsilon \in (0, \varepsilon_0)$ *and* $|k - \frac{1}{2}| < \eta\varepsilon^{\frac{3}{2}}$*.*

Remark 1. *If sign*$(P_0, Q_0) = +1$*, the* ε *neighbourhoods are reversed in Theorem* 2*. That is,* (2) *admits a unique Bloch wave solution for* $\varepsilon \in [0, \varepsilon_0)$ *and three Bloch wave solutions for* $\varepsilon \in (-\varepsilon_0, 0)$*.*

4.1 Analysis Around $k = \frac{1}{2}$

In order to study loops in the Bloch energy band we must consider k slightly perturbed from $k = \frac{1}{2}$ and so take,

$$k = \frac{1}{2} + p, \tag{61}$$

for small p. Consider $\psi(x)$ satisfying (2). ψ can then be expressed as,

$$\psi(x) = e^{ikx}\phi(x) = e^{ipx}e^{\frac{ix}{2}}\phi(x) \equiv e^{ipx}\widetilde{\psi}(x), \tag{62}$$

where $\phi(x+2\pi) = \phi(x)$ as in (3). Then our newly defined $\widetilde{\psi}$ satisfies anti-periodic boundary conditions since,

$$\widetilde{\psi}(x+2\pi) = e^{\frac{ix}{2}} e^{i\pi} \phi(x+2\pi) = -e^{\frac{ix}{2}} \phi(x) = -\widetilde{\psi}(x). \tag{63}$$

Substituting (62) into (2) and replacing $\widetilde{\psi}$ with just ψ gives,

$$\begin{cases} -\psi'' + V(x)\psi + c\psi^3 = (\mu - p^2)\psi + 2ip\psi', & x \in \mathbb{R} \\ \psi(x+2\pi) = -\psi(x), & x \in \mathbb{R} \\ \|\psi\|_{L^2} = 1 \end{cases} \tag{64}$$

our equation of study for this section.

Now consider a neighbourhood of the bifurcation point. Take,

$$c = c_* + \varepsilon, \qquad \mu = \mu_* + M + p^2, \tag{65}$$

where ε and M are small parameters. c and μ (and so ε and M) are related along the branch $\psi(x;c)$ of real-valued stationary solutions. Let us decompose $\psi(x)$ into,

$$\psi(x) = \psi_*(x) + ia\varphi_*(x) + u(x) + iW(x), \tag{66}$$

with $u, W : [-\pi, \pi] \to \mathbb{R}$, $a \in \mathbb{R}$ and $< W, \varphi_* >_{L^2} = 0$. Here we take $\|\psi_*\|_{L^2} = \|\varphi_*\|_{L^2} = 1$, so our normalization condition, $\|\psi\|_{L^2} = 1$, gives,

$$0 = 2 < \psi_*, u >_{L^2} + \|u\|_{L^2}^2 + a^2 + \|W\|_{L^2}^2. \tag{67}$$

Operator L_-^* has a two dimensional kernel, $\mathrm{Ker}(L_-^*) = \{\psi_*, \varphi_*\}$. This motivates us to make the following decomposition, $L^2 = \{\psi_*, \varphi_*\} \oplus \mathrm{Ran}(L_-^*)$ where,

$$\mathrm{Ran}(L_-^*) = \{f \in L^2 : \quad < f, \psi_* >_{L^2} = < f, \varphi_* >_{L^2} = 0\}. \tag{68}$$

We again introduce the projection operator $P_- : L^2 \to \mathrm{Ran}(L_-^*)$ and again will need the norm $\|P_-(L_-^*)^{-1}P_-\|_{\mathcal{H}^2 \to \mathcal{H}^2}$ as well as $\|(L_+^*)^{-1}\|_{\mathcal{H}^2 \to \mathcal{H}^2}$.

Lemma 4. *There exists $N_\pm > 0$ such that,*

$$\|P_-(L_-^*)^{-1}P_-\|_{\mathcal{H}^2 \to \mathcal{H}^2} \leq N_-, \quad \|(L_+^*)^{-1}\|_{\mathcal{H}^2 \to \mathcal{H}^2} \leq N_+.$$

Proof. The norms $\|P_-(L_-^*)^{-1}P_-\|_{\mathcal{H}^2 \to \mathcal{H}^2}$ and $\|(L_+^*)^{-1}\|_{\mathcal{H}^2 \to \mathcal{H}^2}$ are computed in the same manner as the norm in Lemma 1. □

Substituting (66) into (64) and equating the real and imaginary parts yields,

$$(L_+^* + 3\varepsilon\psi_*^2 - M)u = H_+ + N_+(u, W) + K_+(W'; p), \tag{69}$$

$$(L_-^* + \varepsilon\psi_*^2 - M)W = H_- + N_-(u, W) + K_-(u'; p), \tag{70}$$

where,

$$\begin{aligned} H_+ &:= M\psi_* - \varepsilon\psi_*^3, \\ N_+ &:= -(\varepsilon + c_*)((3u^2 + (a\varphi_* + W)^2)\psi_* + (u^2 + (a\varphi_* + W)^2)u), \\ K_+ &:= -2p(a\varphi_*' + W'), \\ H_- &:= Ma\varphi_* - \varepsilon a\psi_*^2\varphi_*, \\ N_- &:= -(\varepsilon + c_*)(2\psi_* u + u^2 + (a\varphi_* + W)^2)(a\varphi_* + W). \\ K_- &:= 2p(\psi_*' + u'). \end{aligned}$$

A further examination of u and W is in order. If each function ψ_*, φ_*, u and W have definite parity, then H_+, N_+ and K_+ have the same parity as ψ_*, u, W' and φ_*' where as H_-, N_- and K_- have the same parity as φ_*, W, u' and ψ_*'. In addition, $L_\pm$ preserves parity. Hence, a unique solution for u, if it exists, must have the same parity as ψ_*, φ_*' and W'. Similarly, if a unique solution for W exists then it must have the same parity as φ_*, ψ_*' and u'. Note that ψ_* and φ_* have opposite parities, which suggests that u and W should continue to have the same parity as ψ_* and φ_* respectively.

Expand u as the following,

$$u = Mu_1 + \varepsilon u_2 + a^2 u_3 + apu_4 + U, \tag{71}$$

where,

$$u_1 := (L_+^*)^{-1}\psi_*, \quad u_2 := -(L_+^*)^{-1}\psi_*^3, \quad u_3 := -c_*(L_+^*)^{-1}\varphi_*^2\psi_*, \quad u_4 := -2(L_+^*)^{-1}\varphi_*'.$$

The normalization condition (67) is further expanded as,

$$\begin{aligned} 0 = 2M < \psi_*, u_1 >_{L^2} + 2\varepsilon < \psi_*, u_2 >_{L^2} + 2a^2 < \psi_*, u_3 >_{L^2} + a^2 + 2ap < \psi_*, u_4 >_{L^2} \\ + \mathcal{O}(\|U\|_{L^2}, \|W\|_{L^2}^2). \end{aligned} \tag{72}$$

Assuming that $< \psi_*, u_1 >_{L^2} = < \psi_*, (L_+^*)^{-1}\psi_* >_{L^2} \neq 0$, then there is a unique solution of (72) for M,

$$M = \alpha_0\varepsilon + \beta_0 a^2 + \gamma_0 ap + \mathcal{O}(\|U\|_{L^2}, \|W\|_{L^2}^2), \tag{73}$$

where,

$$\alpha_0 := -\frac{< \psi_*, u_2 >_{L^2}}{< \psi_*, u_1 >_{L^2}}, \quad \beta_0 := -\frac{1 + 2 < \psi_*, u_3 >_{L^2}}{2 < \psi_*, u_1 >_{L^2}}, \quad \gamma_0 := -\frac{< \psi_*, u_4 >_{L^2}}{< \psi_*, u_1 >_{L^2}}.$$

We shall see later that the $\mathcal{O}(ap)$ term is small enough to ignore. Using (71), we rewrite (69) in the following way,

$$U = (L_+^*)^{-1}(N_+ + c_* a^2 \varphi_*^2 \psi_* + Mu - 3\varepsilon\psi_*^2 u - 2pW') \equiv \mathcal{A}_+(U; W, \varepsilon, a, p). \tag{74}$$

Note that (73) gives us $M = M(\varepsilon, a^2, ap, \|U\|_{L^2}, \|W\|_{L^2}^2)$.

Lemma 5. *$\mathcal{A}_+(U; W, \varepsilon, a, p) : \mathcal{H}^2_{a.p.} \to \mathcal{H}^2_{a.p.}$ has a unique fixed point in a neighbourhood of $0 \in \mathcal{H}^2_{a.p.}$ for small $(W, \varepsilon, a, p) \in \mathcal{H}^2_{a.p.} \times \mathbb{R} \times \mathbb{R} \times \mathbb{R}$ and there exists $D > 0$ such that*

$$\|U\|_{H^2} \leq D(\varepsilon^2 + a^4 + a^2 p^2 + |a|\|W\|_{H^2}). \tag{75}$$

Proof. Again, we appeal to the Banach Fixed Point Theorem [1] by considering a neighbourhood of $0 \in \mathcal{H}^2_{a.p.}$,

$$\bar{\mathcal{B}}_r := \{U \in \mathcal{H}^2_{a.p.} : \|U\|_{\mathcal{H}^2} \leq r\}. \tag{76}$$

One can show, similarly to the proof of Lemma 2, that if $(W, \varepsilon, a, p) \in \mathcal{H}^2_{a.p.} \times \mathbb{R} \times \mathbb{R} \times \mathbb{R}$ are small then $\mathcal{A}_+$ maps $\bar{\mathcal{B}}_r$ into itself and that $\mathcal{A}_+$ is a contraction mapping. □

Now consider the equation for W and rewrite (70) with (71) and (75) as,

$$L_-^* W = (M - \varepsilon\psi_*^2)W + H_- + N_- + K_- \equiv \mathcal{G}(\varepsilon, a, p, W). \tag{77}$$

To have $\mathcal{G} \in \mathrm{Ran}(L_-^*)$ we set the constraints,

$$< \mathcal{G}, \varphi_* >_{L^2} = 0, \quad < \mathcal{G}, \psi_* >_{L^2} = 0, \tag{78}$$

since $\{\varphi_*, \psi_*\} = \mathrm{Ker}(L_-^*)$. Constraint $< \mathcal{G}, \psi_* >_{L^2} = 0$ is satisfied trivially because ψ_* and $\mathcal{G}$ have opposite parities. By expanding constraint $< \mathcal{G}, \varphi_* >_{L^2} = 0$ we obtain,

$$\begin{aligned} 0 =& Ma(1 - 2c_* < \psi_*\varphi_*^2, u_1 >_{L^2}) - c_* a^3(2 < \psi_*\varphi_*^2, u_3 >_{L^2} + \|\varphi_*\|_{L^4}^4) \\ & - \varepsilon a(< \psi_*^2, \varphi_*^2 >_{L^2} + 2c_* < \psi_*\varphi_*^2, u_2 >_{L^2}) + 2p < \psi_*', \varphi_* >_{L^2} \\ & + \mathcal{O}(\varepsilon^2 a, a^5, p^2 a, p\varepsilon, a\|U\|_{L^2}, \varepsilon\|W\|_{L^2}), \end{aligned} \tag{79}$$

where $\|U\|_{L^2}$ is controlled by (75) and M is controlled by (73). As a result, we obtain a relationship between ε, a, p and W:

$$\varepsilon a P_0 + a^3 Q_0 + p R_0 + \mathcal{O}(\varepsilon^2 a, a^5, \varepsilon\|W\|_{L^2}) = 0, \tag{80}$$

with,

$$\begin{aligned} P_0 &:= - < \psi_*^2, \varphi_*^2 >_{L^2} - 2c_* < \psi_*\varphi_*^2, u_2 >_{L^2} + \alpha_0(1 - 2c_* < \psi_*\varphi_*^2, u_1 >_{L^2}), \\ Q_0 &:= -c_*(2 < \psi_*\varphi_*^2, u_3 >_{L^2} + \|\varphi_*\|_{L^4}^4) + \beta_0(1 - 2c_* < \psi_*\varphi_*^2, u_1 >_{L^2}), \\ R_0 &:= 2 < \psi_*', \varphi_* >_{L^2} . \end{aligned}$$

Note that (80) does not provide a unique solution for a (examples will be seen shortly in Sections 4.2-4.4). We want p to be as small as the other terms in (80). Therefore $|p| = \mathcal{O}(a^3) = \mathcal{O}(a\varepsilon)$. Thus, $|ap| = \mathcal{O}(a^4)$ and is negligible in (73). Assuming that $< \psi_*', \varphi_* >_{L^2} \neq 0$ we can solve (80) uniquely for p and eliminate p from further computations.

Now we can solve (77),

$$W = (P_-(L_-^*)^{-1}P_-)\mathcal{G} \equiv \mathcal{A}_-(W; \varepsilon, a), \tag{81}$$

since p is now controlled by (80).

Lemma 6. *$\mathcal{A}_-(W; \varepsilon, a) : \mathcal{H}_{a.p.}^2 \to \mathcal{H}_{a.p.}^2$ has a unique fixed point in a neighbourhood $0 \in \mathcal{H}_{a.p.}^2$ for $(\varepsilon, a) \in \mathbb{R} \times \mathbb{R}$ and there exists $D > 0$ such that,*

$$\|W\|_{H^2} \leq D(|\varepsilon a| + |a|^3). \tag{82}$$

Proof. The proof is similar to the proofs of Lemma 2 and Lemma 5. □

We are now equipped to prove the main theorem.

Proof of Theorem 2. Expansion (73) tells us that the number of branches for μ, as in (65), will depend on the number of admissible values for a in (80). For $p = 0$, the assumption of $\mathrm{sign}(P_0 Q_0) = -1$ implies that for each $\varepsilon \in (-\varepsilon_0, 0]$ (for some ε_0) (80) admits only one solution for a, $a = 0$ and for each $\varepsilon \in (0, \varepsilon_0)$ (80) admits three solutions for a, $a = 0$ and $a = \pm\sqrt{-\varepsilon P_0/Q_0}$. Now consider $p \neq 0$

but small. Note that the p^2 term in (65) is negligible since $|p| = \mathcal{O}(a^3)$. For a fixed $\varepsilon \in (-\varepsilon_0, \varepsilon_0)$ consider the discriminant of (80) given by,

$$\Delta = \Delta(p) = -4Q_0(\varepsilon P_0)^3 - 27(Q_0 p P_0)^2. \tag{83}$$

$\Delta < 0$ for each $\varepsilon \in (-\varepsilon_0, 0]$ since $\text{sign}(P_0 Q_0) = -1$. This is the condition required for (80) to admit one (real) solution in a. For a fixed $\varepsilon \in (0, \varepsilon_0)$ define,

$$p_0(\varepsilon) := \sqrt{\frac{-4\varepsilon^3 P_0}{27 Q_0}}, \tag{84}$$

so that $\Delta(p_0(\varepsilon)) = 0$ and $\Delta(p) > 0$, $\forall p < p_0(\varepsilon)$. Therefore, for all $\varepsilon \in (0, \varepsilon_0)$ (80) admits three solutions for a providing $|k - \frac{1}{2}| = p < p_0(\varepsilon)$. Since different solutions for a in (80) correspond to different Bloch wave solutions in (2), the proof is complete. □

We remark that the arguments in the proof of Theorem 2 could be repeated around $k = 0$ simply by changing the boundary condition in (64) to $\psi(x + 2\pi) = \psi(x)$ and working with $\psi \in \mathcal{H}^2_{per}$. Such is the case in Figure 5 whose configuration satisfies the conditions for bifurcation of the stationary real branch for $c_* > 0$. As for $c_* < 0$ as in Figure 6 the analysis can be repeated as above with $c = c_* + \varepsilon$ and $\mu = \mu_* + M$ so that a loop in the Bloch band will appear when $\varepsilon < 0$ but now under the assumption $\text{sign}(P_0 Q_0) = +1$. The difference for $c_* < 0$ is that this loop will appear upside down when compared to the loops with $c_* > 0$. We note that the side of ε, either $\varepsilon > 0$ or $\varepsilon < 0$, for which we have one or three Bloch wave solutions near $k = 0$ or $k = \frac{1}{2}$ is dependent on the sign of $P_0 Q_0$. We evaluate this sign numerically in Sections 4.2-4.4 and do in fact see the correct orientation of the solution branches. We first present a result pertaining to the sign of P_0.

Lemma 7. *Take $k = 0$ or $k = \frac{1}{2}$. For P_0 defined in* (80) *the following identity holds,*

$$\left.\frac{d\lambda_-^{(n)}}{dc}\right|_{c=c_*} = -P_0, \tag{85}$$

where $\lambda_-^{(n)}$ is the n^{th} eigenvalue of L_- such that $\lambda_-^{(n)} = 0$ for $c = c_*$ and the corresponding eigenfunction at $c = c_*$ is φ_*.

Proof. Take,

$$c = c_* + \varepsilon, \quad \mu = \mu_* + M, \tag{86}$$

as in (65). Consider,

$$L_- = -\partial_x^2 + V(x) + c\psi^2 - \mu, \tag{87}$$

for purely real ψ. Decompose ψ as in (66) but keep only the real parts,

$$\psi = \psi_* + M u_1 + \varepsilon u_2 + \mathcal{O}(\varepsilon^2 + M^2), \tag{88}$$

with u_1 and u_2 defined by (71). Substituting (88) to (87) yields at the leading order,

$$L_- = L_-^* + \varepsilon\psi_*^2 + 2c_*(\psi_* M u_1 + \psi_* \varepsilon u_2) - M + \mathcal{O}(\varepsilon^2 + M^2). \tag{89}$$

The Rayleigh quotient (40) now gives us,

$$\begin{aligned}\lambda_-^{(n)} &=< L_-\varphi_-^{(n)}, \varphi_-^{(n)} >_{L^2} \\ &= \varepsilon < \psi_*^2, \varphi_*^2 >_{L^2} + 2c_* M < \psi_*\varphi_*^2, u_1 >_{L^2} - M + 2c_*\varepsilon < \psi_*\varphi_*^2, u_2 >_{L^2} + \mathcal{O}(\varepsilon^2 + M^2), \end{aligned} \tag{90}$$

once we note that $L_-^*\varphi_* = 0$. We have determined M as a function of ε in (73). Since we are only concerned with real solutions we take here $M = \alpha_0\varepsilon + \mathcal{O}(\varepsilon^2)$. Hence,

$$\left.\frac{d\lambda_-^{(n)}}{dc}\right|_{c=c_*} =< \psi_*^2, \varphi_*^2 >_{L^2} + \alpha_0(2c_* < \psi_*\varphi_*^2, u_1 >_{L^2} - 1) + 2c_* < \psi_*\varphi_*^2, u_2 >_{L^2} = -P_0, \tag{91}$$

the desired result. □

Corollary 2. *If $\lambda_-^{(n)\prime}(c_*) < 0$, that is, the eigenvalue $\lambda_-^{(n)}$ crosses 0 from positive to negative values as c increases, then $P_0 > 0$.*

4.2 Example with $k = \frac{1}{2}$, $n = 0$ and $c_* > 0$

We now illustrate the results of Section 4.1 using the simplest example; the Bloch wave for the lowest energy band, $n = 0$, around $k = \frac{1}{2}$ (Figure 1). For this case, if $V(x) = \cos(x)$, then $c_* = 1$ and $\mu_* = \frac{5}{4}$. As well, ψ_* and φ_* admit closed form solutions [3],

$$\psi_*(x) = \sqrt{2}\sin\left(\frac{x}{2}\right), \qquad \varphi_*(x) = \sqrt{2}\cos\left(\frac{x}{2}\right). \tag{92}$$

We evaluate coefficients S_0, P_0, Q_0, R_0 numerically,

$$S_0 \approx 0.3647, \quad P_0 \approx 0.7419, \quad Q_0 \approx -1.4838, \quad R_0 = -1.$$

We can now solve (80) for a in terms of ε for a fixed value of p. A plot with $p = 0$ and small $p > 0$ is shown in Figure 7. Once we solve for a in terms of ε we can solve for M in terms of ε in (73). Using (65), we plot solution branches on the (c, μ) diagram in Figure 8. Since we have found the relationship between M and ε we can now solve for M as a function of p in (80) and so μ as a function of k from (65) and (61). In this way Figure 9 shows the Bloch bands around $k = \frac{1}{2}$ for values of c close to c_* (small ε).

Let us define,

$$c_+(p) = c_* + \varepsilon_+(p), \tag{93}$$

where, according to (84),

$$\varepsilon_+(p) \approx \sqrt[3]{\frac{-27Q_0p^2}{4P_0}}. \tag{94}$$

Then for $c > c_+(p)$ and for a fixed p, three solution branches exist in (2) according to Theorem 2.

In Figure 7 we see clearly the pitchfork bifurcation of the stationary real branch. Parameter a here represents the magnitude of the imaginary component of ψ. For $p = 0$, red in Figure 7, and $\varepsilon < 0$ we see the only solution has $a = 0$ and so is purely real. For $\varepsilon > 0$ we see the persistence of

the real solution ($a = 0$) and the appearance of two new solution branches with $a \neq 0$. However, the values of a are equal in magnitude and so they represent complex-conjugate solutions with the same eigenvalue, μ. For $p \neq 0$ solutions cannot be purely real. The behaviour described in Theorem 2 is observed as we have one solution branch for $\varepsilon < \varepsilon_+(p)$ and three solution branches for $\varepsilon > \varepsilon_+(p)$.

In Figure 8 a similar behaviour is observed. For $p = 0$ the stationary real branch, as seen numerically in Figure 1a, persists for $c > c_*$ and the appearance of the new (complex) branch is seen at $c = c_*$. For $p \neq 0$ there is one solution branch for $c < c_+(p)$ and three solution branches for $c > c_+(p)$.

Now on to Figure 9. With $c < c_*$ we have a single solution for each k close to $k = \frac{1}{2}$. At $c = c_*$ the band forms a cusp at $k = \frac{1}{2}$ after which, $c > c_*$, we see the appearance of a loop. To show that $k = \frac{1}{2}$ is a cusp point for the band at $c = c_*$ ($\varepsilon = 0$), we note from (65), (73) and (80) that,

$$\left.\frac{d\mu}{dk}\right|_{k=\frac{1}{2}} = \left.\frac{dM}{dp}\right|_{p=0} = 2\beta_0 a \left.\frac{da}{dp}\right|_{p=0} = \frac{2\beta_0}{3}\left(\frac{R_0}{Q_0}\right)^{\frac{2}{3}} \left.\frac{1}{p^{\frac{1}{3}}}\right|_{p=0} = \infty. \tag{95}$$

From Figure 8 one observes that the real solution has a larger eigenvalue, μ, than the complex solution at $k = \frac{1}{2}$ ($p = 0$). So, the solution at the top of the loop corresponds to the real solution. The complex-conjugate solutions are located at the bottom of the loop where the loop intersects itself. The degeneracy stems from the two solutions having the same magnitude of a in Figure 7.

4.3 Example with $k = 0$, $n = 1$ and $c_* > 0$

For this configuration (Figure 5) there is no closed form solution for c_*, μ_*, ψ_* or φ_*. We must therefore approximate these values and functions numerically as in Section 3.2. We implement a root finding scheme on the third eigenvalue of L_- ($m = 2$ in Figure 5c) to find the value $c = c_*$ where this eigenvalue crosses zero. Numerically we compute $c_* \approx 0.3943$ and $\mu_* \approx 1.5155$. Then, ψ_* and φ_* are given as the eigenfunctions of the two zero eigenvalues of L_- at $c = c_*$. Once we approximate ψ_* and φ_* numerically we can compute the normal form coefficients,

$$S_0 \approx 0.8600, \quad P_0 \approx 0.8993, \quad Q_0 \approx -0.7873, \quad R_0 \approx 1.7575.$$

Indeed $\text{sign}(P_0 Q_0) = -1$ as desired. The validity of our numerical computations is addressed in Appendix A.

We plot the bifurcation diagram in Figure 10, the solution branches around the bifurcation point $c = c_*$ in Figure 11 and the Bloch bands in Figure 12. These figures are qualitatively similar to Figures 7-9. Note that the sign of R_0 only changes the bifurcation diagram a versus ε and does not change the actual behaviour of the solution branches.

4.4 Example with $k = 0$, $n = 2$ and $c_* < 0$

For this configuration (Figure 6), we compute, $c_* \approx -0.3237$ and $\mu_* \approx 0.7531$. When the values of c are reduced, it is the second eigenvalue of L_- that crosses zero ($m = 1$ in Figure 6c). Normal form coefficients are found to be,

$$S_0 \approx -0.8733, \quad P_0 \approx 1.3177, \quad Q_0 \approx 0.7787, \quad R_0 \approx -1.8283.$$

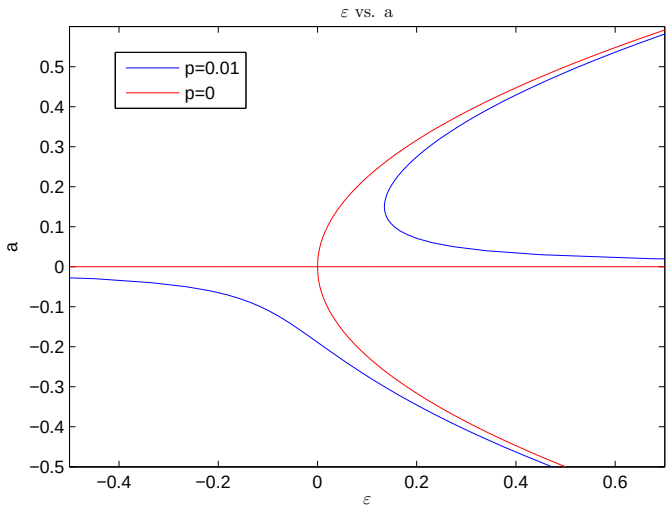

Figure 7: The dependence of a versus ε for $k = \frac{1}{2}$, $n = 0$ and two values of $p = k - \frac{1}{2}$. Here we see a pitchfork bifurcation when $p = 0$. When $p > 0$ the symmetry is broken and the unfolded pitchfork bifurcation is observed.

Note that $\text{sign}(P_0 Q_0) = +1$ which gives three solution branches for $\varepsilon < 0$ or $c < c_* < 0$. Figures 13, 14 and 15 characterize the relevant bifurcation. The Bloch bands as seen on the μ versus k plot in Figure 15 have similar characteristics to Figures 9 and 12, the difference being that the loop appears upside down.

5 Stability of the Pitchfork Bifurcation

Stability of the stationary solutions of (2) will be studied using the same Lyapunov-Schmidt reduction method as in Section 4.1. We keep the discussion brief and only show main results of these computations. To expose the stability of the above stationary solutions we must consider the time-dependent Gross-Pitaevskii equation and so take $\Psi(x,t)$ solving (1). If Ψ is taken in the form,

$$\Psi(x,t) = e^{-i\mu t}\psi(x), \tag{96}$$

then $\psi(x)$ solves the stationary equation (2). Take,

$$c = c_* + \varepsilon, \quad \mu = \mu_* + M(t), \quad k = \frac{1}{2} + p, \tag{97}$$

with ε, $M(t)$ and p small as in the stationary case. We have absorbed the p^2 term into M; it will again be negligible. Decompose $\Psi(x,t)$ as,

$$\Psi(x,t) = e^{-i\mu_* t - i\int_0^t M(\tau)d\tau}(\psi_*(x) + ia(t)\varphi_*(x) + u(x,t) + iW(x,t)). \tag{98}$$

Substituting (98) to (64) and equating the real and imaginary parts gives,

$$(L_+^* + 3\varepsilon\psi_*^2 - M)u = -\dot{a}\varphi_* - W_t + H_+ + N_+(u,W) + K_+(W';p), \tag{99}$$
$$(L_-^* + \varepsilon\psi_*^2 - M)W = u_t + H_- + N_-(u,W) + K_-(u';p). \tag{100}$$

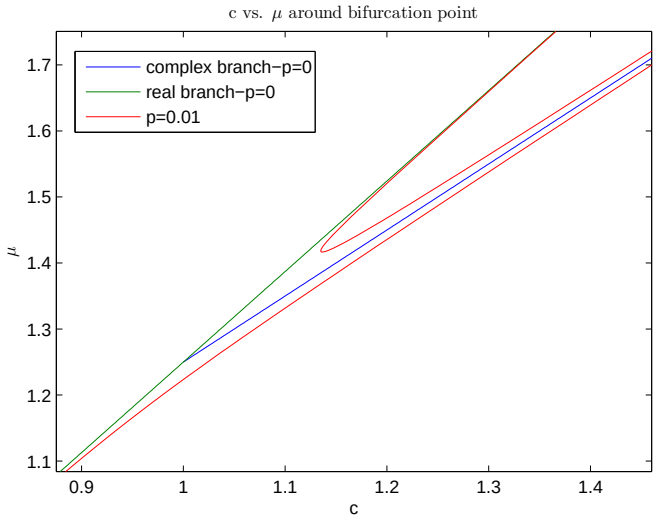

Figure 8: The dependence of μ versus c for $k = \frac{1}{2}$, $n = 0$ and two values of $p = k - \frac{1}{2}$. For $p = 0$ we see the stationary real branch (green), as seen numerically in Figure 1a. The appearance of a new (complex) solution is observed at $c = c_* = 1$. The red curve gives solutions branches for $p \neq 0$. One solution branch is seen for $c < c_+(p)$, where $c_+(p) > c_*$. Three solution branches are observed in a neighbourhood of $c > c_+(p) > c_*$.

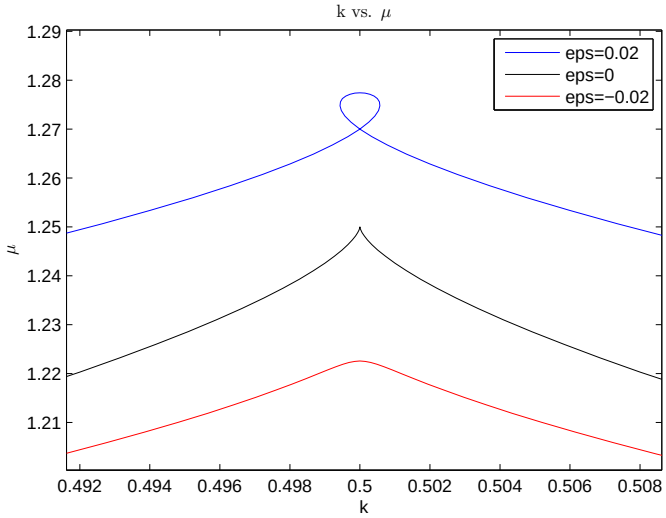

Figure 9: The dependence of μ versus k for $n = 0$ and three values of $c = c_* + \varepsilon$. The transition of the Bloch band through the bifurcation is seen. For $c < c_*$ the curve is smooth. At $c = c_*$ a cusp point forms. Beyond the bifurcation value $c > c_*$ a loop forms in the Bloch band.

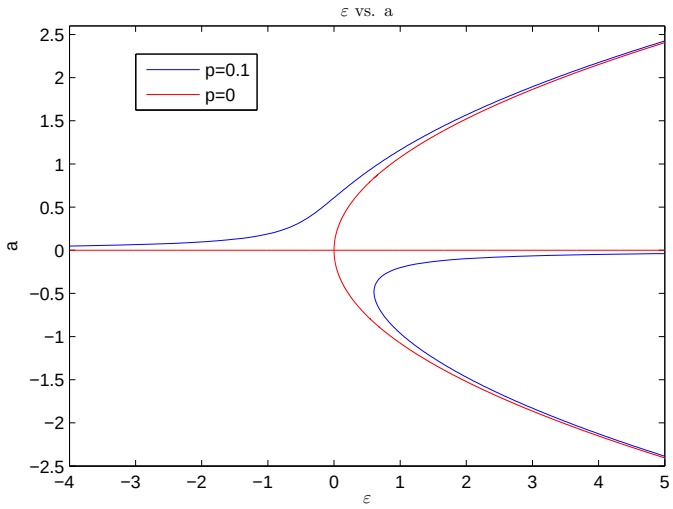

Figure 10: The dependence of a versus ε for $k = 0$, $n = 1$ and two values of $p = k$. Behaviour is similar to Figure 7.

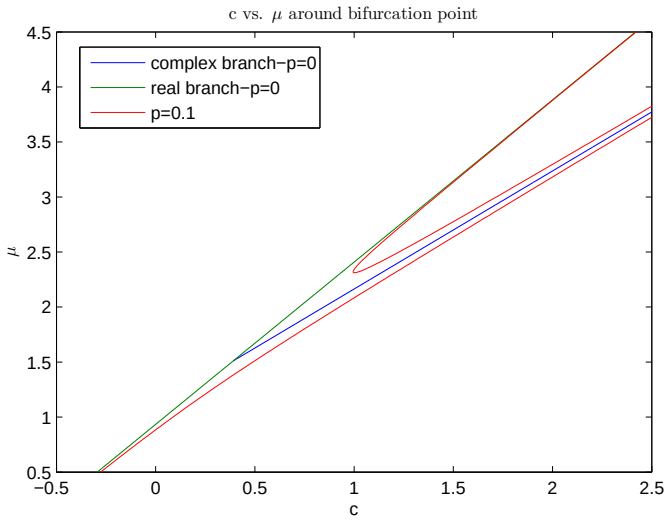

Figure 11: The dependence of μ versus c for $k = 0$, $n = 1$ and two values of $p = k - \frac{1}{2}$. Behaviour is similar to Figure 8.

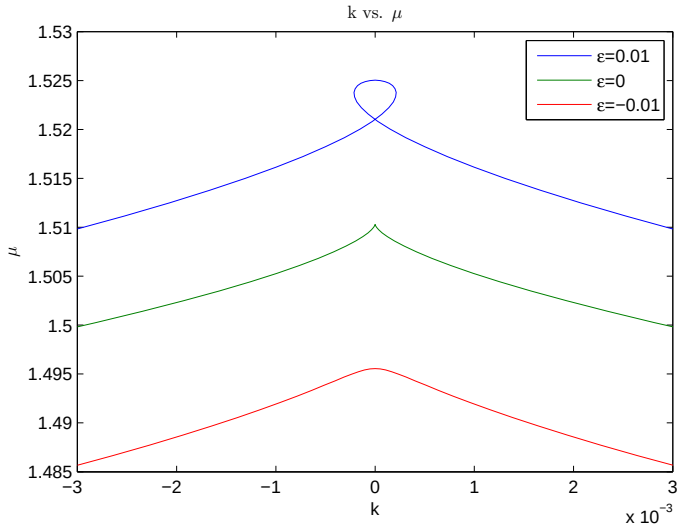

Figure 12: The dependence of μ versus k for $n = 1$ and three values of $c = c_* + \varepsilon$. Behaviour is similar to Figure 9.

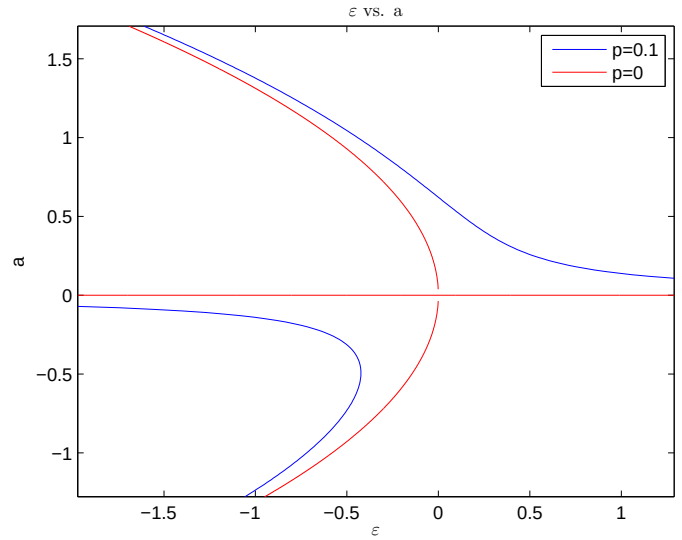

Figure 13: The dependence of a versus ε for $k = 0$, $n = 2$ and two values of $p = k$. Behaviour is similar to Figure 7 just with orientation reversed.

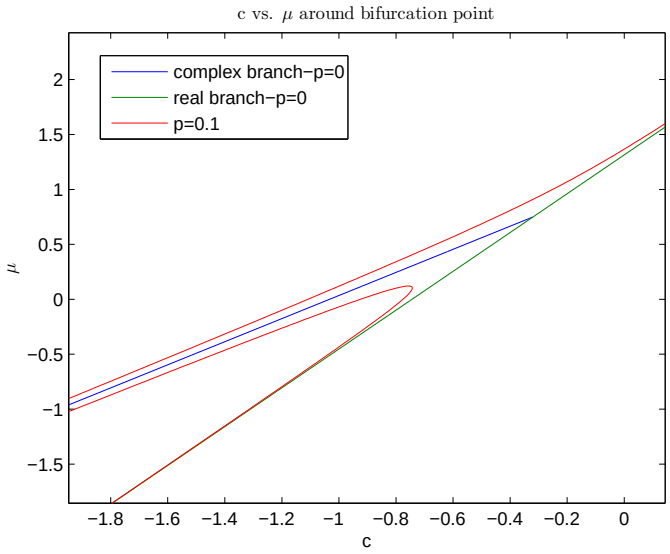

Figure 14: The dependence of μ versus c for $k = 0$, $n = 2$ and two values of $p = k - \frac{1}{2}$. Behaviour is similar to Figure 8 just with orientation reversed.

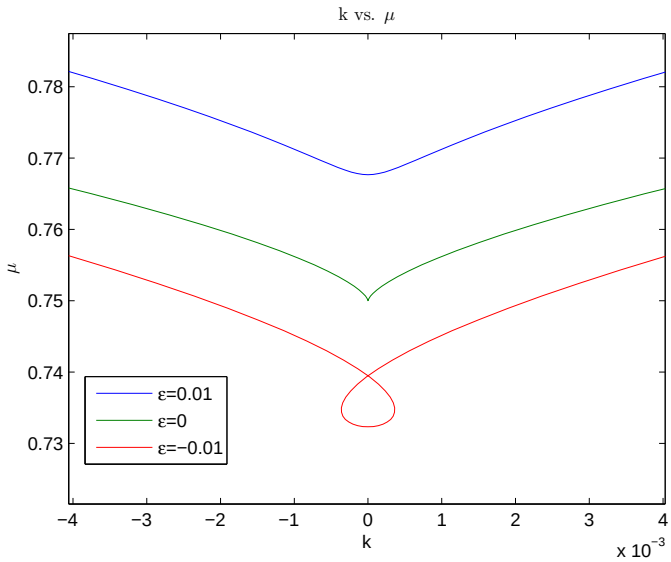

Figure 15: The dependence of μ versus k for $n = 2$ and three values of $c = c_* + \varepsilon$. For $c > c_*$ we have one Bloch band. At the bifurcation value $c = c_*$ a cusp forms in the Bloch band. When $c < c_*$ we see the appearance of a loop structure.

Decompose u as in (71) but with one additional term,

$$u = Mu_1 + \varepsilon u_2 + a^2 u_3 + apu_4 + \dot{a}u_5 + U, \tag{101}$$

where,

$$u_5 := -(L_+^*)^{-1}\varphi_*.$$

The normalization condition, $\|\Psi(\cdot,t)\|_{L^2} = 1$, now reads,

$$0 = 2M < \psi_*, u_1 >_{L^2} + 2\varepsilon < \psi_*, u_2 >_{L^2} + 2a^2 < \psi_*, u_3 >_{L^2} + a^2 + 2ap < \psi_*, u_4 >_{L^2} + \mathcal{O}(\|U\|_{L^2}, \|W\|_{L^2}^2), \tag{102}$$

noting that $< \psi_*, u_5 >_{L^2} = - < \psi_*, (L_+^*)^{-1}\varphi_* >_{L^2} = 0$, thanks to the opposite parity of ψ_* and φ_*. This condition gives the same M as before,

$$M = \alpha_0 \varepsilon + \beta_0 a^2 + \mathcal{O}(|ap|, \|U\|_{L^2}, \|W\|_{L^2}^2). \tag{103}$$

The equation for W (100) now reads,

$$L_-^* W = \mathcal{G}(\varepsilon, a, p, W) + \dot{M}u_1 + 2a\dot{a}u_3 + \dot{a}pu_4 + \ddot{a}u_5 + U_t \equiv \mathcal{E}, \tag{104}$$

where $\mathcal{G}$ is as defined in (77). In order to have $\mathcal{E} \in \mathrm{Ran}(L_-^*)$ we require,

$$\frac{d}{dt} < \psi_*, u >_{L^2} = - < \psi_*, \mathcal{G} >_{L^2} \tag{105}$$

$$\frac{d}{dt} < \varphi_*, u >_{L^2} = - < \varphi_*, \mathcal{G} >_{L^2} . \tag{106}$$

The first constraint (105) is already satisfied because the normalization condition, $\|\Psi(\cdot,t)\|_{L^2} = 1$, is constant in time. The second constraint (106) gives,

$$\ddot{a} < \varphi_*, u_5 >_{L^2} + < \varphi_*, \mathcal{G} >_{L^2} = -\frac{d}{dt} < \varphi_*, U >_{L^2} . \tag{107}$$

Once we note that, $< \varphi_*, u_1 >_{L^2} = < \varphi_*, u_3 >_{L^2} = < \varphi_*, u_4 >_{L^2} = 0$. Expanding at the highest order yields the time-dependent normal form equation,

$$\ddot{a}N_0 + \varepsilon a P_0 + a^3 Q_0 + pR_0 + \mathcal{O}(\varepsilon^2 a, a^5, a\|U\|_{L^2}, \varepsilon\|W\|_{L^2}, \|U_t\|_{L^2}) = 0, \tag{108}$$

where P_0, Q_0 and R_0 are as in (80) and,

$$N_0 := < \varphi_*, u_5 >_{L^2} = - < \varphi_*, (L_+^*)^{-1}\varphi_* >_{L^2} .$$

The justification of (108) hinges on the smallness of $a\|U\|_{L^2}$, $\varepsilon\|W\|_{L^2}$ and $\|U_t\|_{L^2}$, the proof of which is beyond the scope of this project. See [7] for a recent treatment of time-dependent normal forms in the context of nonlinear Schrödinger equations.

Phase portraits for the truncated normal form equation (108) can be obtained by plotting the level curves of the energy equation,

$$E = \frac{\dot{a}^2 N_0}{2} + \frac{\varepsilon a^2 P_0}{2} + \frac{a^4 Q_0}{4} + paR_0, \tag{109}$$

for various values of E. Note that $N_0 < 0$ if $(L_+^*)^{-1}$ is positive definite (as for the lowest energy band, $n = 0$). Indeed, for $n = 0$, $k = \frac{1}{2}$ and $c_* > 0$, the configuration in Section 4.2, we find the numerical value: $N_0 \approx -1.3480$.

Plots for $p = 0$ are seen in Figure 17. Figure 18 shows phase portraits for $p \neq 0$ but small. In Figure 17a, $\varepsilon < 0$, we see that the one equilibrium point at $(0, 0)$ is a center; a stable configuration. In Figure 17b, $\varepsilon > 0$, three equilibrium solutions are present. The solution with $a = 0$ is a saddle point and therefore unstable. The two new solutions, each with the same magnitude of a, are centers and so stable. In Figure 18 we see similar dynamics even though the symmetry of the problem is broken. For $\varepsilon < 0$, Figure 18a, shows one center, so a stable equilibrium. For $\varepsilon > \varepsilon_+(p) > 0$ as seen in Figure 18b, there is again one unstable saddle point and two stable centers, providing p is sufficiently small.

At $k = \frac{1}{2}$ the behaviour observed is exactly that of a supercritical pitchfork bifurcation. The stationary real branch is stable before the bifurcation but loses its stability after the bifurcation as the stable complex-conjugate solutions appear. Away from $k = \frac{1}{2}$ the single branch which exists for $c < c_*$ is stable and remains stable for $c > c_*$. Of the two new branches that appear, as a result of the saddle-node bifurcation, one is stable and the other is unstable. In Figure 7 the branch with the smallest $|a|$ is the unstable branch. This corresponds to the branch in Figure 8 with the largest value for μ. So in Figure 9 the top of the loop is unstable while the bottom of the loop and branch leading up to the loop are stable. Figure 16 illustrates the stability of the Bloch wave solutions at a loop of the energy band.

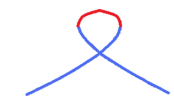

Figure 16: A loop in the energy band for Bloch waves. Red indicates unstable solutions while blue represents stable solutions.

For $n = 1$, $k = 0$ and $c_* > 0$ as in Section 4.3 we numerically compute $N_0 \approx -2.4679 < 0$. Hence phase portraits for this configuration will be qualitatively the same as Figures 17 and 18 and so the stability of the stationary branches will be identical to the case when $n = 0$, $k = \frac{1}{2}$ and $c_* > 0$.

For $n = 2$, $k = 0$ and $c_* < 0$, the configuration in Section 4.4, we find numerically $N_0 \approx 2.5291$. The reversed signs of $N_0 > 0$ and $\text{sign}(P_0 Q_0) = +1$ gives behaviour similar to Figures 17a and 18a before the bifurcation, for $\varepsilon > 0$, as well as similar behaviour to Figures 17b and 18b after the bifurcation for, $\varepsilon < 0$. The stability of the solution branches therefore remains the same. The stationary real branch is stable prior to the bifurcation point $c > c_*$ but becomes unstable for $c < c_*$. The new complex-conjugate branches are stable when they appear.

6 Conclusion

To summarize, stationary Bloch waves of the Gross-Pitaevskii equation were studied in a periodic potential. It was proved that the stationary real solutions are uniquely continued from from the linear limit. Numerical and asymptotic results indicated that the stationary real branch will undertake a bifurcation when an eigenvalue of the linearization operator L_- changes sign. The spectrum of L_- was computed numerically to observe this behaviour.

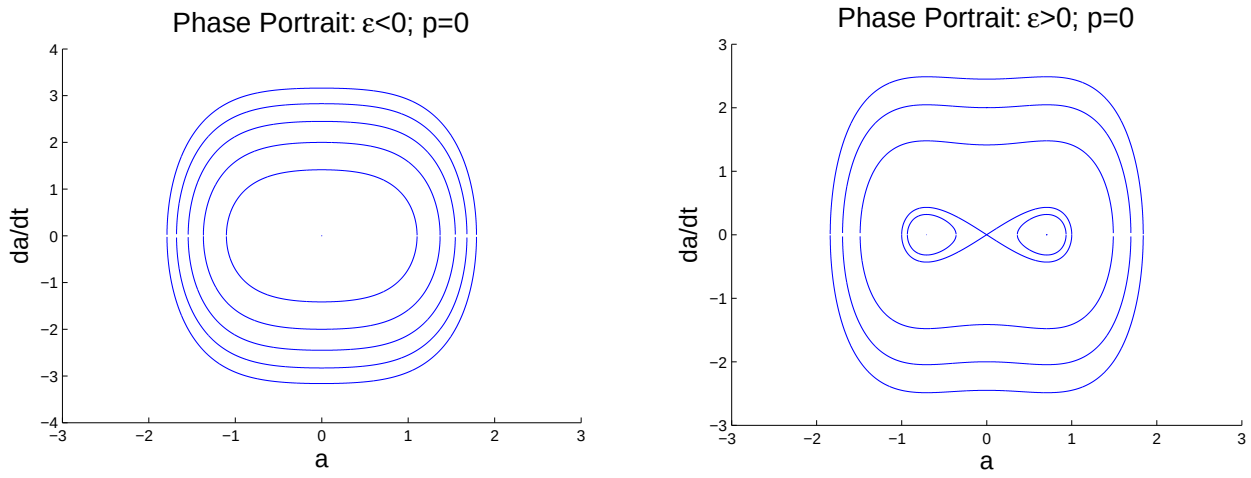

(a) (b)

Figure 17: Phase portraits for $p = 0$. (a) $\varepsilon < 0$: one equilibrium; center. (b) $\varepsilon > 0$: three equilibria; two centers and one saddle.

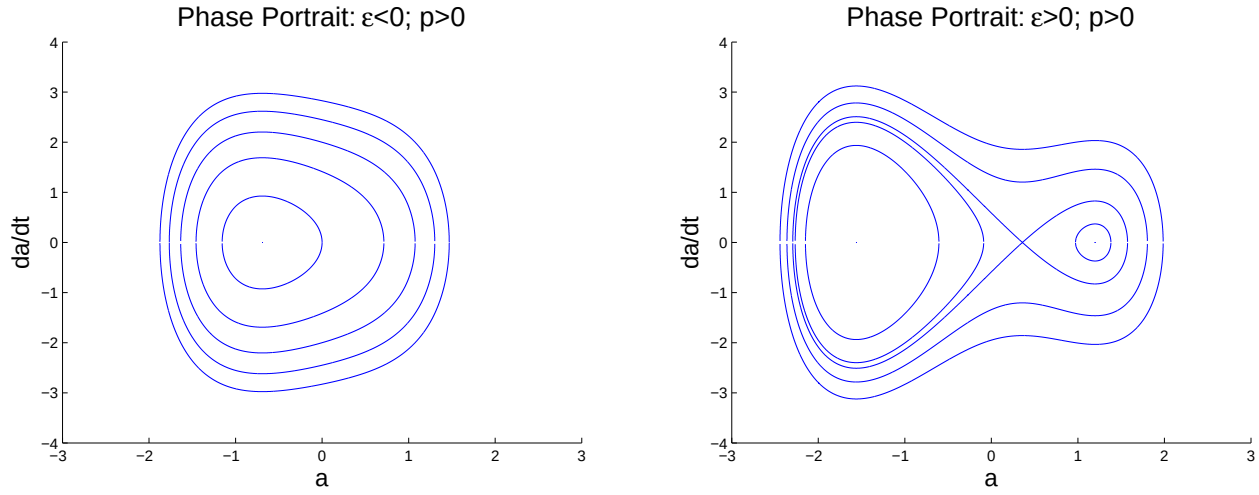

(a) (b)

Figure 18: Phase portraits for $p \neq 0$. (a) $\varepsilon < 0$: one equilibrium; center. (b) $\varepsilon > 0$: three equilibria; two centers and one saddle.

The bifurcation of the stationary real branch was studied analytically using the Lyapunov-Schmidt reduction method and was revealed to be a pitchfork bifurcation. The analysis led to a normal form equation which exposed the qualitative behaviour of the system around the bifurcation point. This behaviour was illustrated numerically in specific examples.

Finally, the stability of the stationary states was examined. The stationary real branch was found to be stable before the bifurcation point after which it loses its stability. The new complex-conjugate solutions were found to be stable as they appeared. The stability of solutions along a loop in the energy band was also established.

A Numerical Error

The analytical solutions for c_*, μ_*, ψ_* and φ_* when $k = \frac{1}{2}$ and $n = 0$ as outlined in Section 4.2 present an excellent opportunity to check our numerical methods. Bifurcation values c_* and μ_* are approximated numerically from roots of the second eigenvalue of operator L_- on Figure 1c, for varying step sizes. The distance of these numerical values c_{num} and μ_{num} from the exact values $c_* = 1$ and $\mu_* = \frac{5}{4}$ is shown on Figure 19. We can observe a slow (linear) convergence of numerical approximations.

We can also compare the numerical approximations of the solution ψ_{num} (computed from the shooting method) and the eigenfunction of L_-^*, φ_{num} (computed with an eigenfunction solver) with the exact functions ψ_* and φ_*. Figure 20 shows the errors in the supremum ℓ^∞ norms. We again see the linear convergence of numerical approximations. Note that the error is smaller for the output of the shooting method when compared to the eigenfunction solver.

References

[1] E. Zeidler, *Applied functional analysis: main principles and their applications*. Springer-Verlag, New York, 1995.

[2] J. C. Bronski, L. D. Carr, B. Deconinck, J. N. Kutz and K. Promislow, Phys. Rev. E **63**, 036612 (2001).

[3] B. Wu and Q. Niu, New Journal of Physics **5**, 104.1-104.24 (2003).

[4] M. Machholm, C. J. Pethick and H. Smith, Phys. Rev. A **67**, 053613 (2003).

[5] B. P. Venkatesh, M. Trupke, E.A. Hinds, and D.H.J. O'Dell, Phys. Rev. A **80**, 063834 (2009).

[6] B. P. Venkatesh, J. Larson, and D.H.J. O'Dell, *Band structure loops and multistability in cavity-QED*, arXiv:1101.1570 (2011).

[7] D. Pelinovsky and T. Phan, *Normal form for the symmetry-breaking bifurcation in the nonlinear Schrödinger equation*, arXiv:1101.5402 (2011).

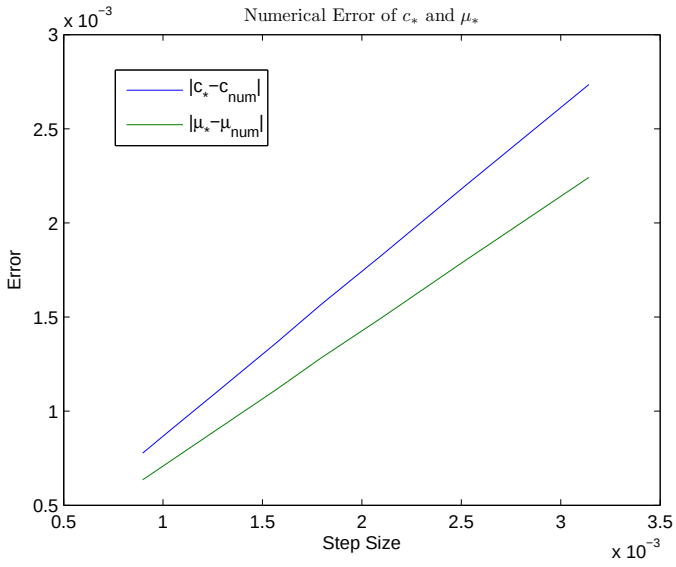

Figure 19: Numerical error of finding c_* and μ_* as a function of step size.

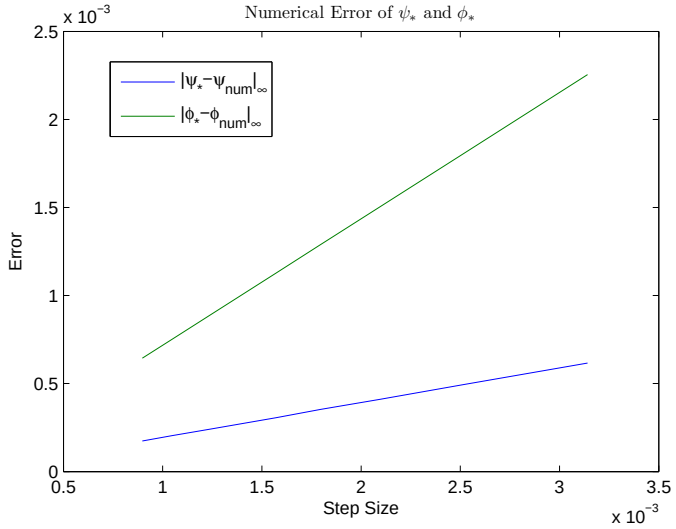

Figure 20: Numerical error of finding ψ_* and φ_* as a function of step size.